



**HAL**  
open science

## Comparing the sorption kinetics of poly-tetrafluoroethylene processed either by extrusion or spark plasma sintering

Ilham Elaboudi, Ahmed Mdarhri, Christian Brosseau, Ali Nourdine, Mourad  
Rzaizi, Laurent Servant

► **To cite this version:**

Ilham Elaboudi, Ahmed Mdarhri, Christian Brosseau, Ali Nourdine, Mourad Rzaizi, et al.. Comparing the sorption kinetics of poly-tetrafluoroethylene processed either by extrusion or spark plasma sintering. *Polymer*, 2020, 190, pp.122192. 10.1016/j.polymer.2020.122192 . hal-02548877

**HAL Id: hal-02548877**

**<https://hal.science/hal-02548877>**

Submitted on 7 Mar 2022

**HAL** is a multi-disciplinary open access archive for the deposit and dissemination of scientific research documents, whether they are published or not. The documents may come from teaching and research institutions in France or abroad, or from public or private research centers.

L'archive ouverte pluridisciplinaire **HAL**, est destinée au dépôt et à la diffusion de documents scientifiques de niveau recherche, publiés ou non, émanant des établissements d'enseignement et de recherche français ou étrangers, des laboratoires publics ou privés.



Distributed under a Creative Commons Attribution - NonCommercial 4.0 International License

1 **Comparing the sorption kinetics of poly-tetrafluoroethylene processed either by**  
2 **extrusion or spark plasma sintering**

3 **Ilham Elaboudi<sup>a</sup>, Ahmed Mdarhri<sup>a</sup>, Christian Brosseau<sup>b</sup>, Ali Nourdine<sup>c</sup>, Mourad Rzaizi<sup>a</sup>**  
4 **and Laurent Servant<sup>d</sup>**

5 <sup>a</sup>Faculty of Sciences & Techniques, Cadi Ayyad University, LMCN, A. Khattabi Marrakech  
6 BP 549, 40 000, Morocco

7 <sup>b</sup>Univ Brest, CNRS, Lab-STICC, UMR CNRS 6285, CS, 93837, 6 avenue Le Gorgeu, 29238,  
8 Brest Cedex 3, France

9 <sup>c</sup>Université Grenoble Alpes, Université Savoie Mont Blanc, CNRS, Grenoble INP (Institute of  
10 Engineering Univ. Grenoble Alpes), LEPMI, UMR CNRS 5279, 38000, Grenoble, France

11 <sup>d</sup>Université de Bordeaux, Institute of Molecular Sciences, Group of Molecular Spectroscopy,  
12 UMR CNRS 5255, BP 351, Cours de la Libération, Talence, France

13  
14  
15 **Abstract**

16  
17 The key goal of this study was to compare the sorption kinetics properties of poly-  
18 tetrafluoroethylene (PTFE) processed either by spark plasma sintering (SPS-PTFE) or  
19 extrusion methods (Ext-PTFE). A gravimetric-sorption technique was used to obtain kinetic  
20 and equilibrium adsorption data at room temperature in several liquids (toluene, n-hexane,  
21 tetrahydrofuran and chloroform). Sorption kinetics was quantified using the Berens-  
22 Hopfenberg empirical model. The results are discussed in terms of liquid diffusion and  
23 polymer relaxation. An attempt was made to correlate the crystallization rate, apparent  
24 diffusion coefficient and sorption rate for the series of samples. Additionally, the effect of  
25 sorption kinetics on the structure and mechanical properties of PTFE samples was  
26 investigated. Swelling of SPS-PTFE reduces slightly the crystallite thickness, the Young's  
27 modulus and yield stress. In contrast, the crystalline phase is less impacted by swelling for  
28 Ext-PTFE samples for which Young's modulus is increased under the combined effect of  
29 swelling and tensile stress.

30  
31  
32  
33

## 34 1. Introduction and overview

35

36 PTFE is a synthetic fluoropolymer used in numerous industrial applications (it is often  
37 referred by its trade name Teflon). The production of PTFE is forecast to continue to increase  
38 over the course of the next ten years [1]. The demand arises because PTFE combines various  
39 excellent properties: chemical resistance, high temperature stability, favorable mechanical  
40 properties and low permittivity [2]. Such unique characteristics made PTFE widely used in  
41 automotive, electrical, and electronic industries, aircraft and aerospace, communications,  
42 construction, medical devices and implants stents, special packaging, and protective garments  
43 [2,3]. Additionally, PTFE has outstanding permeability properties making it relevant for  
44 sealing and in compounds for transferring aggressive or ultrapure fluids such as pipe liners,  
45 fittings, valves, and pumps [3-5].

46 However, PTFE is difficult to process by using conventional thermoplastics methods, such as  
47 extrusion-molding or injection- molding [3,6,7]. These methods require heating PTFE powder  
48 until complete melting (380°C), and during this stage, PTFE can be subject to oxidation, i.e.  
49 degradation. Additionally, its high viscosity in the molten state makes shaping difficult and  
50 restricts the use of filler particles which can be embedded into a PTFE matrix [3,8]. During  
51 the cooling phase, volumetric changes associated with crystallization and density difference  
52 between the crystalline and amorphous phases produce shrinkage [9]. Metallurgy techniques  
53 such as hot pressing (HP), hot isostatic press (HIP), or high velocity compaction (HVC) have  
54 been applied to process PTFE powder but these methods present many drawbacks [10,11],  
55 e.g. high pressures and high temperatures are needed. Moreover, during the compaction  
56 process, the material undergoes very large permanent strains inducing pore heterogeneities  
57 and residual stresses within the compact as well as local texture of the nascent crystalline  
58 phase [12-14]. After compaction, the sintered material is heated above the melting  
59 temperature before being cooled. During this heat treatment, complex mechanisms induce  
60 anisotropic deformations by growth and expansion of the polymer micro-particles.  
61 Furthermore, rates of sintering are limited ( $\approx 10^\circ\text{C}/\text{min}$ ) and require a long processing time,  
62 i.e. typically a few hours. An innovative method was tested recently to prevent such problems  
63 and overcome those limitations by using an advanced metallurgic technique named spark  
64 plasma sintering (SPS) [13-15]. This method is a solid consolidation sintering process and  
65 consists in apply simultaneously a low voltage, high density pulse current and uniaxial  
66 pressure to the powder particles. This heating mechanism is beneficial to the process since  
67 heating takes place at the contact between powder and sintering tool. Thus, it concentrates

68 sintering energy on the contact necks of powder particles and renders the process energy  
69 economic and easy to control.

70 The key advantages offered by this sintering method include high densities achieved in a short  
71 time (typically a few minutes), high sintering rate (up to 400°C/min) at low temperatures or  
72 below melting temperature for some polymeric materials [16], and decrease of particle growth  
73 during processing [15,16].

74 Until today, SPS was applied to process ceramic and metallic materials [10,11] and  
75 few work has been devoted to polymeric materials and composites [17-20]. Polyimide and  
76 polyetheretherketone (PEEK) powders were sintered using SPS process [17]. Authors  
77 reported that optimizing the sintering conditions (compressive load, heating and cooling rate,  
78 pulse current density, dwell time) has a strong impact on the physical properties of the  
79 sintered polymers, specifically of the density and mechanical properties (Young's modulus,  
80 yield strength, maximum compressive strain). For instance, PEEK with improved mechanical  
81 properties was obtained by SPS below the melting temperature, compared to PEEK obtained  
82 with the conventional injection molding technique [16].

83 In previous studies [15,20], the mechanical properties of PTFE processed by SPS have  
84 been investigated. The results were in agreement with those published in the archival  
85 literature for PTFE fabricated by standard method. Given the importance of SPS processing  
86 variables (rate of heat, temperature of sintering, pressure, dwell time), SPS could have some  
87 advantage to improve polymer quality and reduce the manufacturing time and cost.  
88 **Complementary to examining its mechanical characteristics, we believe it is of paramount**  
89 **importance to investigate other physical and chemical properties of SPS-PTFE in order to**  
90 **compare them with PTFE manufactured by ordinary methods. These characteristics include**  
91 **permeability properties, notably for its use in vascular graft applications as well as other**  
92 **surgical procedure requiring a long-term dimensional stability [4].**

93 This manuscript reports and compares **the swelling properties** and kinetics of solvent  
94 diffusion in PTFE elaborated by extrusion (hereafter denoted as Ext-PTFE) and SPS  
95 (hereafter denoted as SPS-PTFE samples). It is long established that the transport  
96 phenomenon in polymers depends on the nature of the penetrant and on the polymer structure  
97 in combination with the processing method [21,22]. Our central aim is to bring more detailed  
98 understanding **of the impact of the processing method on the sorption kinetics of PTFE.** For  
99 this purpose, different liquids were tested: toluene, n-hexane, tetrahydrofuran (THF) and  
100 chloroform. Sorption kinetics was investigated using Berens-Hopfenberg (BH) empirical  
101 model [23].The results are discussed in terms of diffusion and polymer relaxation

102 phenomenon. An attempt was made to correlate the liquid properties, polymer characteristics  
 103 (interaction free energy, Hansen parameters solubility, crystallinity) and fitting parameters  
 104 (diffusion coefficient, relaxation or Fickian diffusion contribution) of our modeling method.  
 105 Furthermore, the swollen polymers were subjected to additional analysis by infrared  
 106 spectroscopy, X-ray diffraction and uniaxial tensile tests in order to study the effect of  
 107 sorption on the structure and mechanical properties of the samples depending on the  
 108 processing method.

109

## 110 2. Experimental section

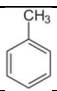
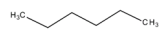

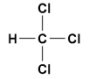
### 111 2.1. Materials

112

113 Industrial grade PTFE was used to perform the experiments. On the one hand, **Ext-PTFE**  
 114 **samples were purchased from Guarniflon Society**, of density 2.18 g/cm<sup>3</sup>. On the other hand,  
 115 SPS samples were obtained by using PTFE powder provided by the Hoechst-Germany  
 116 company (Hostaflon TF1620) and an HP 25/1 machine from FCT system GmbH (Germany).  
 117 The size distribution of the PTFE particles was obtained from SEM observations by  
 118 dispersing PTFE powder in a suitable solvent (2-propanol). The average value of particle  
 119 diameter is found to be about 5.44±0.61 μm according to a log-normal distribution [15]. The  
 120 crystallinity degree of the as-received PTFE powder is about 65% measured by DSC method.  
 121 To distinguish the various contributions to the interfacial wettability, we employed different  
 122 types of contacting liquids (purchased from Sigma Aldrich): toluene, tetrahydrofuran, n-  
 123 hexane, and chloroform. Several of their physical properties are listed in Table1.

124

125 **Table 1:** Molar mass, density and molar volume of solvents used for PTFE swelling [24].

Solvent	Structure	Molar mass (g/mol)	Density (g/cm <sup>3</sup> )	Molar volume (cm <sup>3</sup> /mol)
Toluene		92.14	0.867	106.29
N-Hexane		86.18	0.655	131.6
Tetrahydrofuran		72.11	0.888	81.57
Chloroform		119.38	1.489	80.67

126

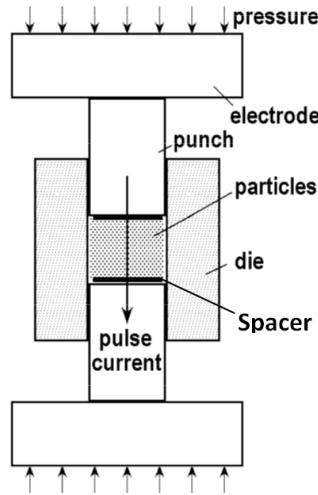
127

## 128 2.2. SPS processing

129

130 The experimental set-up describing the SPS technique is shown in Fig. 1. It is composed of  
131 four parts: the DC generating DC pulsed current via two electrodes, an hydraulic system  
132 providing the uniaxial compaction force by means of two counter sliding punches, the  
133 electrical resistance heating part under vacuum ( $< 2\text{mbar}$ ) and the water cooling chamber. All  
134 elements of the set up (die, punches, electrodes, spacers) are made of conductive graphite.  
135 During processing, 15g of PTFE powder was placed in a die having a cylindrical shape (40  
136 mm and 60 mm as inner and outer diameters respectively). The sintering temperature, heating  
137 rate and the compact force were controlled (Fig. 2). The value of the electric current used to  
138 activate the micro-powder material was fixed to 2 kA with a low voltage value (2 V)[15]. At  
139 the beginning (phase I in Fig.2), and at the cooling step (phase IV in Fig. 2), the sample is  
140 subjected to an uniaxial compaction force of 30 MPa exerted by counter-sliding punches and  
141 through two graphitic spacers. This pressure is sufficient to sinter PTFE powder at room  
142 temperature since it exceeds the yield strength of PTFE (typically ranging from 9 MPa and 12  
143 MPa [15,25]). The die was heated at  $340^{\circ}\text{C}$  and with heating rate  $200^{\circ}\text{C}/\text{min}$  (phase II). The  
144 holding time at this temperature was 1min (phase III) and the cooling rate to attain the  
145 ambient temperature was  $1^{\circ}\text{C}/\text{s}$  (phase IV). To reach the prescribed temperature cycle, the  
146 pulse current was automatically adjusted by controlling the sample temperature using a  
147 thermocouple (positioned in the graphitic die at 3-4mm from the sample side). Direct  
148 temperature measurements at the edge and the center of the sample during heating revealed  
149 the presence of a temperature gradient within the polymer [14]. At the end of the sintering, the  
150 dense polymer has a circular disk shape with 40 mm diameter and 4 mm thickness. Tested  
151 PTFE samples were cut as small rectangular pieces from the processed polymers. The  
152 thickness, length and width of the tested pieces were measured using a high-grade digital  
153 caliper. Dimensions of tested samples are  $50\times 10\times 2$  mm for the Ext-PTFE sample and  
154  $40\times 4\times 1$ mm for SPS-PTFE sample.

155

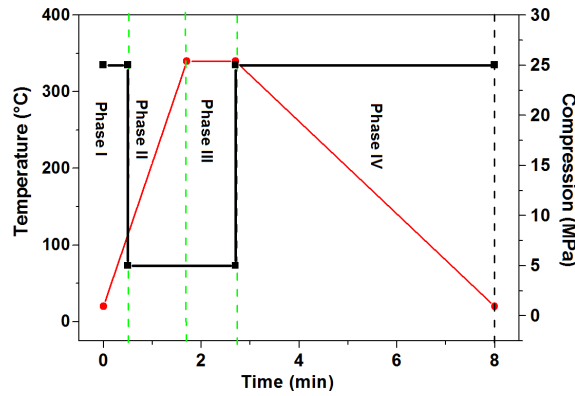


156

157

158

**Fig.1:** Principle of the SPS apparatus.



159

**Fig. 2:** Typical operating conditions for the SPS applied to PTFE powder.

160

161

### 162 2.3. Sorption experiment

163

164 Sorption experiments were carried out by immersing the processed PTFE in the pure liquid at  
 165 room temperature. In order to measure the mass change of PTFE with time, a sensitive  
 166 balance was used with accuracy of  $\pm 0.1\text{mg}$ . The swollen sample was withdrawn from the  
 167 liquid at different values of time  $t$  and weighed ( $m_t$ ) after removing excess surface liquid  
 168 carefully by absorbent paper. In order to eliminate systematic errors, each sample was  
 169 weighed four times and average values were taken. Sorption experiments were continued until  
 170 saturation, corresponding to their equilibrium swelling value ( $m_e$ ). The overall time duration  
 171 for each set of measurements was typically 1000 hours. The swelling ratio ( $Q_t$ ) and  
 172 equilibrium uptake ( $Q_e$ ) were determined by using Eq.(1(a)) and Eq.(1(b)), respectively

173

$$Q_t = \frac{m_t - m_0}{m_0} \times 100 \quad (1-a),$$

174

$$Q_e = \frac{m_e - m_0}{m_0} \times 100 \quad (1-b).$$

175  
176  
177  
178  
179  
180  
181  
182  
183  
184  
185  
186  
187  
188  
189  
190  
191  
192  
193  
194  
195  
196  
197  
198  
199  
200  
201  
202  
203  
204  
205  
206  
207  
208  
209  
210

## 2.4. Contact angle measurement

The hydrophobicity of Ext-PTFE and SPS-PTFE was carried out in terms of static contact angle of water and several liquids (toluene, n-hexane, THF and chloroform). Contact angles were measured at room temperature 20°C and ambient relative humidity 52% using an optical meter EasyDrop KRUSS and rectangular polymers samples. A water droplet with 1mm diameter was dropped on the surfaces of samples from a distance of 1 cm by vibrating the tip of a micro-syringe. The drop image was taken by an integrated camera and analyzed with the number of three measuring cycles, and the average value was recorded as the final contact angle result.

## 2.5. XRD and FTIR characterizations

Ext-PTFE and SPS-PTFE samples in the dry state or saturated by liquids were analyzed by X-ray Diffraction (XRD) and Infrared (IR) spectroscopy. Before measurement, rectangular-shaped (5x5x0.5 mm<sup>3</sup>) samples were conditioned in liquids at room temperature until saturation is occurred. Then, the excess surface solvent was removed by absorbent paper just before characterization by XRD and IR spectroscopy. The crystalline structure of neat and swollen PTFE samples was analyzed by XRD using PHILIPS X'PERT apparatus. The source of irradiation was Cu K $\alpha$  ( $\lambda = 1.5418\text{\AA}$ ). The XRD patterns of samples were recorded from 10° to 50° (2 $\theta$ ). The ATR spectra of the samples were measured using the PLATINUM Diamond ATR accessory and VERTEX 70 FT-IR spectrometer. 20 scans were made at a resolution of 2cm<sup>-1</sup> for spectral accumulation in every measurement.

## 2.6. DSC measurement

The thermal transitions; melting and crystallization of PTFEs were investigated. The experiments were carried out with a PerkinElmer Series 7 differential scanning calorimeter (DSC) at a heating and cooling rate of 10°C/min. The DSC instrument was calibrated with Indium and Zinc as temperature calibration standards. Samples were subjected to a one thermal cycle ranging from 30 °C to 400°C. The first melting event provided the enthalpy of the crystals formed during the cooling after extrusion (Ext-PTFE) or sintering (SPS-PTFE), while the second melting event refers to the crystals formed during the cooling in the DSC. Melting enthalpies were calculated by integration of the endothermic peaks and were used to estimate the degree of crystallinity.



211

## 212 **2.7. Tensile measurement**

213

214 Tensile tests of dry and swollen PTFE samples were performed at room temperature using an  
215 Instron 3369 testing machine. Samples had a square cross section and dimensions as follows:  
216 for Ext-PTFE: 10×2×50mm, and SPS-PTEF: 5×2×40mm. All measurements were performed  
217 at room temperature and at a fixed cross-head speed displacement (1mmmin<sup>-1</sup>). The  
218 mechanical stress history was identical for all dry and swollen samples. Because of the  
219 possible evaporation of the solvent when swollen PTFE samples are subjected to high  
220 deformations for a long time, the maximal strain ( $\epsilon_{\max}$ ) value was fixed to 50%.

221

222

## 223 **3. Modeling solvent sorption kinetics**

224

225 The sorption kinetics of polymers in a low molecular weight liquid has been studied  
226 extensively. A standard model for mass diffusion kinetics is based on the second Fick's law. It  
227 is known in the archival literature as case I or Fickian diffusion and is represented by Eq.(2)

$$228 \quad \frac{\partial C}{\partial t} = -D \frac{\partial^2 C}{\partial x^2} \quad (2),$$

229

230 where  $C$  is the solvent concentration,  $x$  denotes the distance from the sample center,  $D$  is the  
231 diffusion coefficient, and  $t$  is time. If we assume that the surface concentration attains its  
232 equilibrium value  $C_{\infty}$  immediately when it is exposed to solvent and remains constant through  
233 diffusion process, the initial and boundary conditions are given by

$$234 \quad \begin{aligned} t=0^-, \quad C=0, \quad -l/2 \leq x \leq l/2 \\ t \geq 0^+, \quad C=C_{\infty} \quad x=\pm l/2 \end{aligned} ,$$

235

236 where  $l$  is the half-depth of a sample. If  $M_t$  denotes the total amount of diffusing substance  
237 which entered the sample at time  $t$  and  $M_{\infty}$  the corresponding quantity at saturation, the  
238 solution of Eq.(2) using the boundary conditions is given by [26,27]

239

$$240 \quad \frac{M_t}{M_{\infty}} = 1 - \left( \frac{8}{\pi^2} \right) \sum_{n=0}^{\infty} \left[ \left( \frac{1}{(2n+1)^2} \right) \exp \left( - \frac{D(2n+1)^2 \pi^2}{4l^2} t \right) \right] \quad (3).$$

241

242 In Eq.(3), the thickness of the polymer is  $2l$ , and  $D_i$  is the diffusion coefficient. At short times,  
243 Eq. (3) approximates to [27]

244  
245  
246  
247  
248  
249  
250  
251  
252  
253  
254  
255  
256  
257  
258  
259  
260  
261  
262  
263  
264  
265  
266  
267  
268  
269  
270  
271

$$\frac{M_t}{M_\infty} = 2 \left( \frac{D_i t}{\pi l^2} \right)^{1/2} \quad (4).$$

Equation 4 allows us estimating the diffusion coefficient  $D_i$ . For a non-Fickian behavior and  $M_t/M_\infty < 0.5$ , the diffusion coefficient can be calculated using Eq.(4). In this case  $D_i$  reflects the diffusion rate at the first stage of sorption (initial diffusion). According to many reports [28-31], a considerable deviation from ideal Fickian diffusion has been observed where the diffusion rate changes as function of time. This anomalous behavior arises as a direct consequence of the glass transition temperature depletion in these systems called also plasticization. As was interpreted by Roger *et al.* [29], plasticization is interrelated to the finite rate by which changes in polymer structure occur in response to stresses imposed by the medium during sorption. The nature of this glass transition is as yet far from being fully understood and no general theory actually exists dealing with anomalous diffusion in polymers [27,29]. Features of non Fickian diffusion are pointed out by applying a more general empirical law to fit sorption kinetic data

$$\frac{M_t}{M_\infty} = k.t^n \quad (5).$$

In Eq.(5),  $k$  is a constant and depends on the polymer structural properties. The value  $n=0.5$  indicates a Fickian diffusion (Case I) occurring when the polymer matrix is not perturbed by the solvent and the diffusion coefficient of the solvent is independent of the solvent concentration within the duration of the sorption experiment. The value  $n=1$  indicates (case II) diffusion for which the rate of polymer relaxation is faster than the diffusion rate. The polymer is affected and plasticized by the solvent and the diffusion coefficient depends on the local solvent concentration. A value of  $n$  ranging between 0.5 and 1 indicates an anomalous transport or a two-stage behavior and occurs when polymer relaxation and diffusion rates are close. If  $n$  ranges between 0 and 0.5, the diffusion process is called pseudo-Fickian and is considered as well as an anomalous behavior. As reported by Berens and Hopfenberg [31] for non-Fickian diffusion, the incremental sorption shows larger relative contributions from the slow relaxation process. This phenomenon is related to the slow redistribution of available free volume through the relatively large scale segmental motions in the relaxing polymer.

272  
273  
274  
275  
276

Thus, it delays the rate of approach to equilibrium but increases the overall sorption. In order to analyse the pseudo-Fickian diffusion behavior, Berens and Hopfenberg (BH) suggested an empirical model [23,31] based on the linear superposition of Fickian diffusion, Eq.(7), and relaxation processes, Eq.(8),

$$\frac{M_t}{M_\infty} = \frac{M_F}{M_\infty} + \frac{M_R}{M_\infty} \quad (6)$$

277

$$\frac{M_F}{M_\infty} = \alpha_F \left( 1 - \sum_{n=0}^{\infty} \frac{8}{(2n+1)^2 \pi^2} \exp\left(-\frac{(2n+1)^2 \pi^2 D}{L^2} t\right) \right) \quad (7)'$$

$$\frac{M_R}{M_\infty} = \alpha_R [1 - \exp(-k_R t)] \quad (8)$$

278  
279  
280  
281  
282  
283  
284  
285  
286  
287

where  $\alpha_F$  and  $\alpha_R$  denote the mass fractions of uptake in the overall sorption attributed to Fickian diffusion and relaxation phenomenon, respectively,  $k_R$  is the first-order time constant associated with the long time drift in mass uptake and controlled by the viscoelastic relaxation of the polymer chains to accommodate the penetrant. Thus, BH model provides as well a means for calculating a meaningful diffusion coefficient from sorption data involving long term relaxations which may overshadow the rapid achievement of the Fickian diffusion [31,32]. In order to optimize correctly the three unknown parameters ( $\alpha_F$ ,  $k_R, D$ ) in Eq.(7), their effect on the sorption kinetic profile needs first to be evaluated, and the initial iteration values need to be carefully selected.

## 288 4. Results and discussion

289

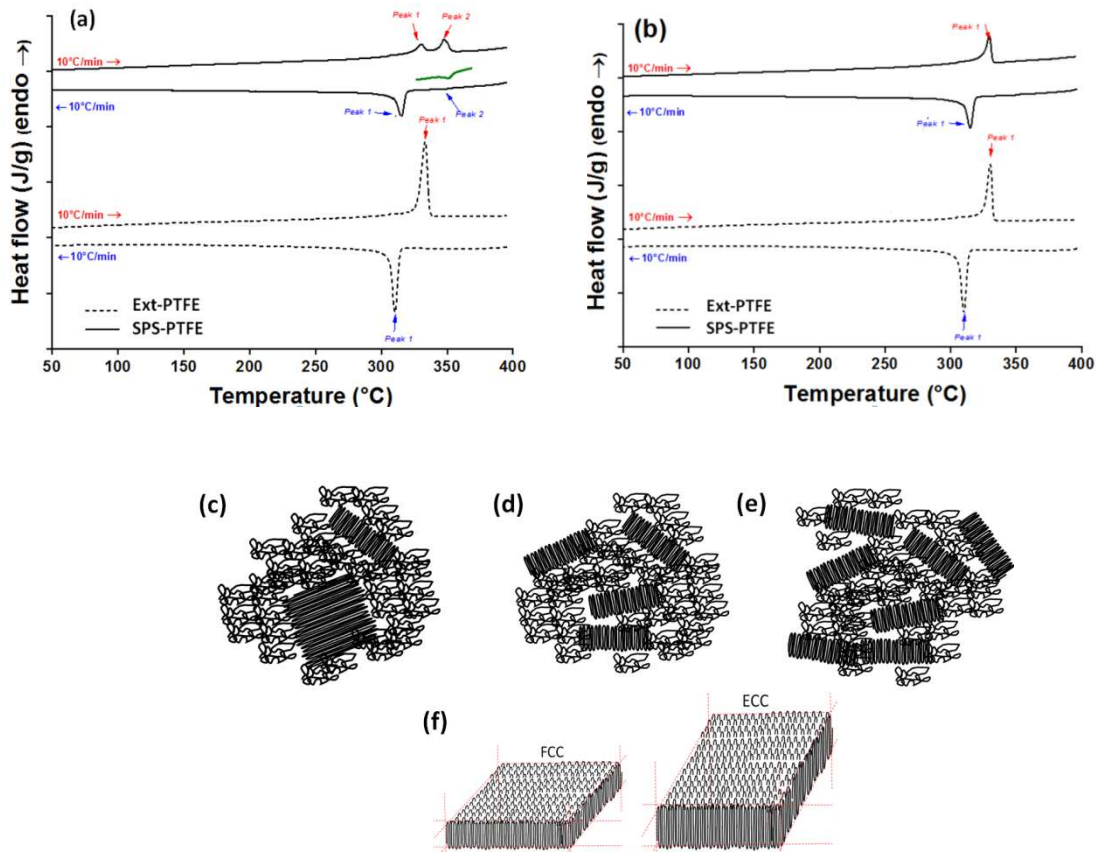
### 290 4.1. Crystallinity of PTFE samples

291

292 The thermograms depicted in Fig.3 show the transitions of Ext-PTFE and SPS-PTFE samples  
293 in the temperature range 30-400°C. A summary of the melting, crystallization peaks  
294 temperatures and heats of fusion are given in Table 2. In the first cycle of heating-cooling, the  
295 Ext-PTFE exhibits a peak of melting at 333°C and provides a total heat of fusion 45J/g. In  
296 case of SPS-PTFE, double melting peaks are observed at 330°C and 348°C. The  
297 corresponding endothermal enthalpies of fusion are about 10.4 and 9.3 J/g respectively. Peaks  
298 observed at lower temperatures for both samples are assigned to the melting of folded chain  
299 crystals (FCC) [33,34]. The melting temperature of FCC in EXT-PTFE is the highest, it could  
300 be assumed that crystallites in these PTFEs differ by size and probably by density of packing,  
301 their increase induce an increase in the melting temperature of FCC [35-37]. The second peak  
302 observed in SPS-PTFE at 348°C can be associated to the melting of the extended chain

303 crystals (ECC) which are perfect and well known for their superheatability [33-36]. Multiple  
304 melting peaks are observed only after melting-recrystallization-next melting cycles of pristine  
305 polymer. Indeed, in [15], a single melting peak at a high temperature 351°C is observed in the  
306 DSC traces of pristine PTFE powder [15]. At the cooling step of the first cycle, crystallization  
307 of melted SPS-PTFE occurs at temperature peak 319°C but a high temperature crystallization  
308 peak shoulder is also observed at 349°C. It is possible that a very low fraction of the crystals  
309 persists to melting to about 400°C and exists in the liquid crystalline state as it was proved in  
310 case of high level orientation of PTFE molecular chains [38]. This state reduces the free  
311 energy barrier to nucleation and crystallization occurs at lower degree of super-cooling [34].  
312 In the second cycle, the high melting peak temperature is absent after recrystallization of SPS-  
313 PTFE. It is supposed that after heating up to 400°C (first cycle), all high ordered crystalline  
314 regions (ECC) disappear, and crystallization during cooling (1<sup>st</sup> cycle) starts with folded  
315 chains nucleus. This is followed by the addition of more segments through a chain folding  
316 process. Because of kinetic barrier, these chains cannot sufficiently adjust their conformations  
317 from folding to straight to form a thermodynamic equilibrium state, i.e., ECC [34]. In the 2<sup>nd</sup>  
318 cycle of heating-cooling, the melting peak temperature of Ext-PTFE shifts from 333 to 330  
319 °C. This indicates that the crystals formed during 1<sup>st</sup> cooling still far from equilibrium. It  
320 could also signify that crystals formed during extrusion are larger in size compared to that of  
321 recrystallized Ext-PTFE (first cycle cooling phase).

322  
323  
324  
325  
326  
327  
328  
329



330  
331  
332

333  
334

335 **Fig.3:** DSC traces of the (a) first and (b) second heating-cooling cycle of Ext-PTFE and SPS-PTFE  
336 (Heating and cooling rate = 10°C/min). Scans are separated on the vertical scale for clarity of  
337 presentation. **Schematics of the mixed amorphous crystalline structure of SPS-PTFE at: (c) the first**  
338 **and (d) second heating/cooling cycles. (e) Same for Ext-PTFE at both cycles. The schematics in (f)**  
339 **illustrates the chain folded crystal structure (FCC) and the extended chains crystal structure (ECC).**

340  
341

342 **Table 2:** Melting peak temperature  $T_m^{\text{peak}}$ , Heat of fusion  $\Delta H_f$ , Crystallization temperature  
343  $T_c^{\text{peak}}$ , crystallization enthalpy  $\Delta H_c$ , Degree of crystallinity  $X_c$  deduced from DSC Scans

344

Material Designation	Cycle number	$T_m^{\text{peak}}$ (°C)	$\Delta H_f$ (J/g)	$X_c$ (%)	$T_c^{\text{peak}}$ (°C)	$\Delta H_c$ (J/g)
SPS-PTFE	1 <sup>st</sup>	330	10.4	24.0	319	-19.8
		348	9.3		349	-0.23
SPS-PTFE	2 <sup>nd</sup>	330	20.7	25.2	315	-22.2
Ext-PTFE	1 <sup>st</sup>	333	45	54.9	310	-0.23
Ext-PTFE	2 <sup>nd</sup>	330	31	37.8	310	-34.2

345  
346

















347 The crystallinity degree of PTFE samples was calculated using  $\chi_c = (\Delta H_m / \Delta H_{m,\infty}) \times 100\%$ , where  
348  $\Delta H_m$  is the measured melting enthalpy and  $\Delta H_{m,\infty}$  is the melting enthalpy of 100% crystalline  
349 PTFE [37,39,40]. Assuming that  $\Delta H_{m,\infty}$  is 82 J/g for PTFE [39,40], the degrees of crystallinity

350 are 54.9% and 24% for Ext-PTFE and SPS-PTFE samples, respectively. The low crystallinity  
 351 of SPS-PTFE was expected because the sample was cooled at a high rate (60°C/min) at the  
 352 phase IV of the SPS process (Fig.2).

#### 353 4.2. Wettability of PTFE surfaces

354  
 355 In order to evaluate the interfacial wettability of PTFE samples and to distinguish the various  
 356 contributions, we employed a series of contacting liquids. Table 3 shows static contact angle  
 357 of Ext-PTFE and SPS-PTFE samples ranging in nature from polar aprotic to nonpolar protic:  
 358 a) water, b) toluene, c) n-hexane, d) THF, e) chloroform, and from the most polar to the less  
 359 polar: water, glycerol, ethanol, diiodomethane.

360  
 361 **Table 3:** Dispersion  $\gamma^d$  and polar  $\gamma^p$  surface tension of liquids (mJ/m<sup>2</sup>) and their contact angles  
 362 (C.A) with PTFEs  
 363

	(a) Water	Glycerol	Ethanol	Di-iodo- methane	(b) Toluene	(c) n-hexane	(d) THF	(e) Chloroform
$\gamma^d$ (mJ/m <sup>2</sup> )	21.6	34	18.8	49.5	28.5	18.4	24.6	25.9
$\gamma^p$ (mJ/m <sup>2</sup> )	51.0	30	2.6	1.3	0	0	0	1.6
$\gamma_l$ (mJ/m <sup>2</sup> )	72.6	64	21.4	50.8	28.5	18.4	24.6	27.5
C.A. Ext-PTFE	107±3 	107±5 	31±2 	88±3 	40±1 	~0±0 	41±2 	39±2 
C.A. SPS-PTFE	116±3 	104±3 	31±3 	84±4 	38±2 	~0±0 	38±1 	36±4 

364  
 365  
 366 The values of the water contact angle for the two kinds of samples are close to each other in  
 367 agreement with the large hydrophobicity of PTFE [41]. For other used liquids (b,c,d,e),  
 368 contact angles are less than 90° indicating that wetting of the PTFE surface is favorable [42],  
 369 which can be assigned to the low liquid surface free energy according to Young equation [43].

370  
 371 To provide an understanding of the **interfacial free energy (IFE)** of PTFE samples, the Owens-  
 372 Wendt approach was chosen since it takes into consideration the sorption of liquid on polymer  
 373 surface which depends on various interfacial interactions between the liquid and the polymer  
 374 phases. This approach proposes that the IFE can be described by a sum of independent  
 375 components: dispersive terms (e.g. London forces arising from the electron dipole fluctuations  
 376 within the molecule) and polar components (e.g. van der Waals forces and hydrogen  
 377 bonding). Owens and Wendt [43] have proposed the following expressions

378

$$1 + \cos \theta = \frac{2}{\gamma_l} \left( \sqrt{\gamma_s^d \gamma_l^d} + \sqrt{\gamma_s^p \gamma_l^p} \right)$$

379

$$\gamma_{sl} = \gamma_s + \gamma_l - 2\sqrt{\gamma_s^d \gamma_l^d} - 2\sqrt{\gamma_s^p \gamma_l^p} \quad (10),$$

$$\gamma_s = \gamma_s^d + \gamma_s^p \quad \text{and} \quad \gamma_l = \gamma_l^d + \gamma_l^p$$

380

381 where  $\gamma_s^d, \gamma_l^d, \gamma_s^p, \gamma_l^p$  are the dispersive and polar components of surface free energy of the solid  
 382 and liquid phases,  $\gamma_{sl}$  is the IFE corresponding to the solid-liquid interface, and  $\theta$  is the  
 383 contact angle for the probe liquid on the solid phase.

384 Unknowns are the polar and dispersive components of PTFEs. They were calculated from  
 385 contact angle measurements using more than two liquids with known polar and dispersive  
 386 components (Table3) [44,45]: water, glycerol, ethanol and diiodomethane in addition to  
 387 toluene, n-hexane, THF and chloroform [46,47]. **Details of calculations are given in appendix**  
 388 **A.**

389 Table 4 shows that **the free surface energy (FSE)** of different processed PTFE samples are  
 390 close to each other and similar to those reported in literature [48]. The polar surface energy of  
 391 SPS-PTFE is slightly higher. This difference could arise from many factors such as roughness  
 392 and porosity [42,45,49].

393

394

**Table 4: FSE** and surface tension components of Ext-PTFE and SPS-PTFE

395

	Ext-PTFE	SPS-PTFE
$\gamma^p(\text{mJ/m}^2)$	0.45±2 .6	1.77±3.2
$\gamma^d(\text{mJ/m}^2)$	18.49±0.63	18.49±0.33
$\gamma_s(\text{mJ/m}^2)$	19±3	20±4

396

397

398 Figure 4 shows the IFE of Ext-PTFE and SPS-PTFE. It decreases progressively from water,  
 399 toluene, THF, n-hexane and Chloroform. Furthermore, IFE of each liquid in contact with Ext-  
 400 PTFE is slightly lower than SPS-PTFE counterpart; this will approve spreading, wetting and  
 401 sorption of liquid in Ext-PTFE.

402

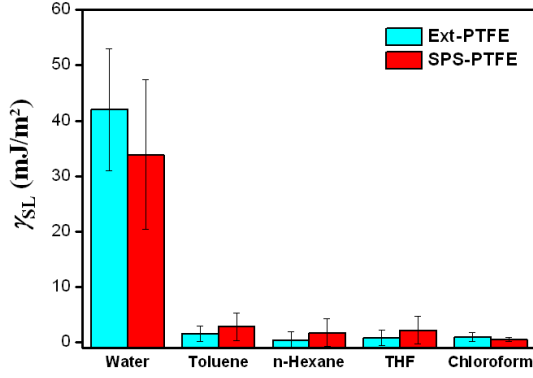


Fig.4: Free energy at the interface liquid/polymer.

### 4.3 Hansen solubility parameters

The Hansen solubility parameters (HSP) are physicochemical parameters, and are widely used to estimate the type of interactive forces responsible for compatibility between materials [50-52]. It predicts the affinity between a couple of polymer and solvent on which the swelling degree depends.

Briefly stated, the basis of the HSP is the assumption that the cohesive energy ( $E$ ) might be divided into three parts corresponding to atomic dispersion ( $E_D$ ), molecular dipolar interactions ( $E_P$ ), and hydrogen-bonding interactions ( $E_H$ ). Similarly, the total Hansen parameter  $\delta_T^2$  can be divided into three components corresponding to the dispersion ( $\delta_D^2 = E_D/V$ ), polar ( $\delta_P^2 = E_P/V$ ) and hydrogen bonding ( $\delta_H^2 = E_H/V$ ) by using  $\delta_T^2 = E/V = \delta_D^2 + \delta_P^2 + \delta_H^2$ , where  $V$  denotes the molar volume of liquid. Using the HSP, the compatibility between two materials can be represented as the relative energy density (RED) which is the ratio between the solubility parameter distance ( $R_a$ ) and the interaction radius ( $R_0$ ) of the polymer.  $R_a$  is defined as

$$R_a^2 = 4(\delta_{D2} - \delta_{D1})^2 + (\delta_{P2} - \delta_{P1})^2 + (\delta_{H2} - \delta_{H1})^2 \quad (11).$$

Further, a radius of interaction  $R_0$  is needed (set to 3.9 for PTFE [44]). If  $RED \leq 1$ , compatibility between the two materials is highly likely. If  $RED \geq 1$ , the two materials will not be compatible and there cannot be wetting between the two materials. The HSP and  $R_a$  values for the four liquids and PTFE [44] are listed in Table 5.



432 **Table 5:** Hansen solubility parameters (HSP) of liquids and equilibrium uptake for SPS-PTFE and  
 433 Ext-PTFE samples.

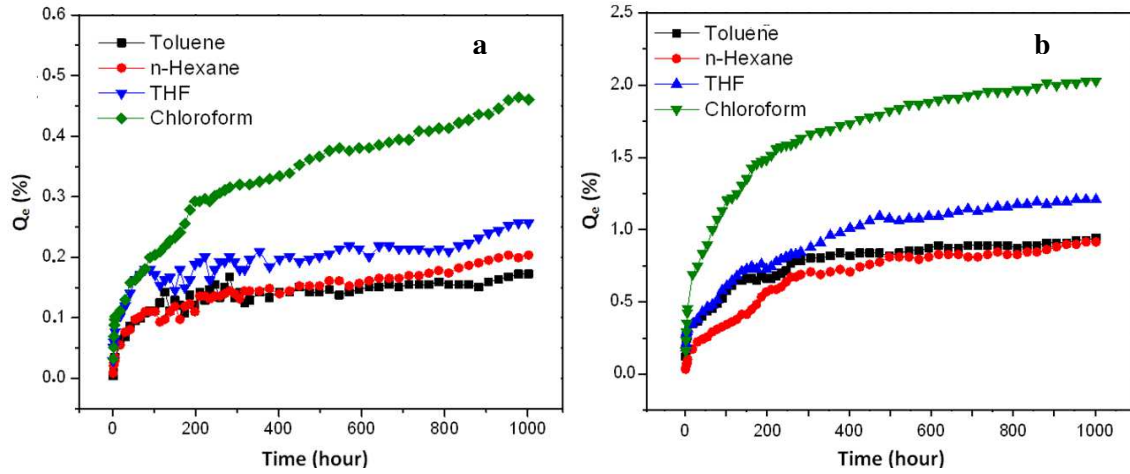
Material	Total HSP (cal/cm <sup>3</sup> ) <sup>1/2</sup>	HSP (cal/cm <sup>3</sup> ) <sup>1/2</sup>			$R_a$ (cal/cm <sup>3</sup> )	RED	$Q_e$ (%)	
	$\delta_T$	$\delta_D$	$\delta_P$	$\delta_H$			Ext-PTFE	SPS-PTFE
Water	14.8	7.4	10	8.1	20	5.12	-	-
Toluene	18.2	18	1.4	2	3.88	0.99	0.17	0.91
n-hexane	14.9	14.9	0	0	4.64	1.19	0.20	0.95
THF	19.5	16.8	5.7	8	6.15	1.58	0.25	1.21
Chloroform	18.9	17.8	3.1	5.7	4.15	1.06	0.46	2.03
PTFE	16.7	16.2	1.8	3.4	$R_0=3.9$	-	-	-

434  
 435 The compatibility between PTFE and the solvent progressively increased from THF, n-  
 436 hexane, chloroform and toluene. It is important to highlight that to achieve effective wetting,  
 437 the surface tension of the surface to be wetted should be higher than the surface tension of the  
 438 material that will wet it. The surface tension of a material depends on the secondary bond  
 439 energy, and there are correlations between the surface tension and the solubility parameters.  
 440 These correlations involve molar volume of liquid molecules [53]. Thus, the HSP data above  
 441 are compatible with the wetting observations shown in Fig.4.

#### 442 4.4. Sorption kinetics

443  
 444 The swelling ratio  $Q_t = \frac{m_t - m_0}{m_0} \times 100$  as function of time is shown in Fig.5. For all sorption  
 445 experiments,  $Q_t$  increases with time until an equilibrium value (equilibrium uptake  $Q_e$ ) is  
 446 reached. The saturation uptake of Ext-PTFE samples are less than 1%. The rate of sorption  
 447 and equilibrium uptake are different for each studied liquid but a general trend is observed,  
 448 i.e. for all PTFE samples investigated,  $Q_e$  increases in the following order: chloroform>THF  
 449 and is similar for n-hexane and toluene (right columns of Table 5).

450



**Fig.5:** Sorption kinetics of liquids for: (a)Ext-PTFE and (b)SPS-PTFE samples.

The swelling behavior of PTFE is conveniently determined by fitting  $M_t/M_\infty$  versus  $t$  using Eq.(5) [29,30]. The results are shown in Table 6 and indicate that the sorption kinetics of Ext-PTFE and SPS-PTFE samples by the tested liquids are pseudo-Fickian in nature, i.e.  $n < 0.5$ .

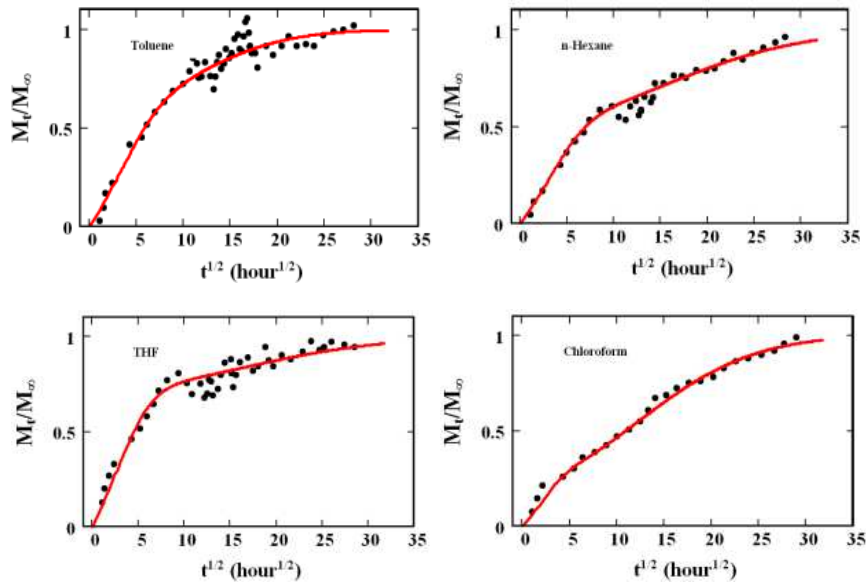
**Table 6:** Calculated diffusion parameters from fit parameters to sorption kinetics curves using the BH empirical power law and Eq.(4).

liquid	$D_t(\text{m}^2/\text{s})$	$K_F=(\pi^2 D_t/l^2)\times 10^5(\text{s})$	$k$	$n$
Ext-PTFE				
toluene	$1.45 \cdot 10^{-11}$	3.63	$0.22\pm 0.02$	$0.22\pm 0.01$
n-hexane	$3.72 \cdot 10^{-12}$	0.93	$0.13\pm 0.01$	$0.29\pm 0.01$
THF	$1.12 \cdot 10^{-11}$	2.78	$0.24\pm 0.01$	$0.20\pm 0.01$
chloroform	$1.07 \cdot 10^{-11}$	2.68	$0.10\pm 0.01$	$0.33\pm 0.01$
SPS-PTFE				
toluene	$2.65 \cdot 10^{-12}$	2.65	$0.21\pm 0.01$	$0.23\pm 0.01$
n-hexane	$5.15 \cdot 10^{-13}$	0.52	$0.08\pm 0.07$	$0.38\pm 0.01$
THF	$1.13 \cdot 10^{-12}$	1.13	$0.13\pm 0.01$	$0.30\pm 0.01$
chloroform	$2.32 \cdot 10^{-12}$	2.32	$0.17\pm 0.01$	$0.26\pm 0.01$

The data above indicate that the experimental data cannot be fitted using a Fickian model, i.e. Eq.(3). To provide a clearer understanding of the trends in sorption kinetics observed for our samples, we examined the behavior of  $M_t/M_\infty$  versus  $t^{1/2}/l$  (where  $l$  denotes sample thickness) in Figs.6 and 7. A linear part of the curve is observed only at the very beginning of the sorption experiments. It indicates that the diffusion is dominated by a rapid Fickian diffusion at the

469  
470  
471  
472  
473  
474  
475  
476  
477  
478  
479  
480  
481  
482  
483  
484  
485  
486  
487  
488  
489  
490  
491  
492

initial stage of swelling for which polymers are solvent- free [30,54]. This linearity allows us estimating the value of the initial diffusion coefficient  $D_i$  by using Eq.(4). To deal with differences in samples thickness  $l$ , an apparent diffusion time  $K_F = (\pi D/l^2)$  was calculated (Table 7). For toluene, n-hexane, THF and chloroform, it is observed that the values of  $K_F$  are smaller in SPS-PTFE compared to Ext-PTFE samples indicating a slower liquid diffusion at the beginning of sorption. What is remarkable is that the opposite trend is observed for the final swelling equilibrium  $Q_e$  values of SPS-PTFE which are found to be the largest. The observed slowing of the initial diffusion for SPS-PTFE compared to Ext-PTFEs originates from its higher IFE and non uniform densification of PTFE powder originating during the sintering process. Indeed, achieving an **homogeneous temperature distribution during sintering is of major concern for the SPS process. The main parameters influencing the temperature gradient inside the specimen include the powder's electrical conductivity, the wall thickness of the die, the presence of graphite papers in contact with the powder, and the temperature dependent thermal and electrical properties of the applied tool materials as well as the powder compact [10,11]. Many authors describe and demonstrate the benefit of making use of an optimized pressing tool system [11], or the so-called hybrid system to reduce the observed thermal gradient [10].**

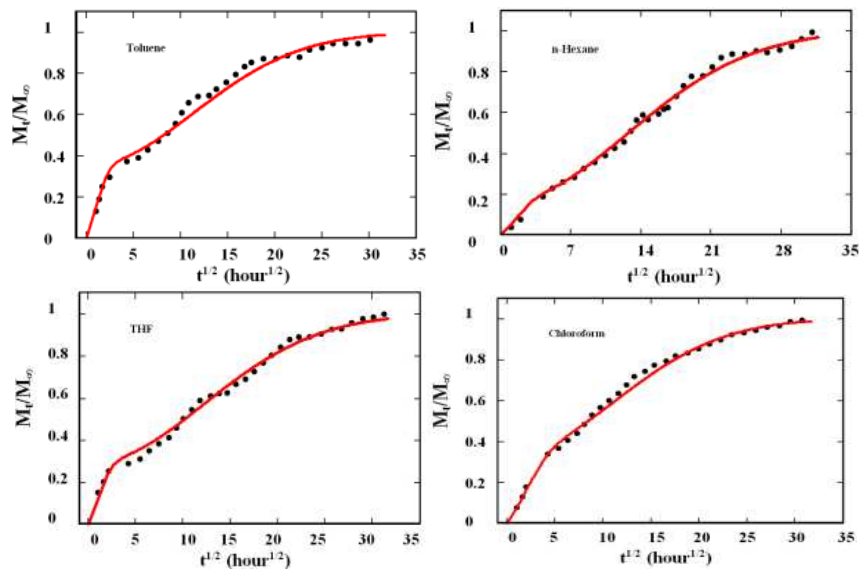


493

494  
495

496

**Fig.6:** A comparison for our sorption kinetics measurements to the BH model for Ext-PTFE samples (the red line shows the fit to the BH model).



497

498  
499

**Fig.7:** Same as in Fig. 6 for SPS-PTFE samples.

500

501 To enable detailed characterization of the true diffusion coefficient over the entire duration of  
 502 sorption experiments, Eqs.(6-8) were used. As shown in Figs. 6 and 7, the BH model  
 503 equations can simulate the kinetic absorption behaviors and also help to rationalize the  
 504 experimental results. The Fickian and relaxation fit parameters are summarized in Table 7.  
 505 Overall, these results indicate that the polymer relaxation contribution is dominant for SPS-  
 506 PTFE samples in contrast to Ext-PTFE samples for which transport is mainly controlled by  
 507 Fickian diffusion with the exception of chloroform.

508 **Table 7:** Calculated diffusion parameters from fit parameters to sorption kinetics curves using  
 509 BH model in both SPS-PTFE and Ext-PTFE samples.

510

Sample processing method	liquid	$\alpha_F$	$D \times 10^{12}$ (m <sup>2</sup> /s)	$K_F = D/l^2 \times 10^5$ (s <sup>-1</sup> )	$K_R \times 10^5$ (s <sup>-1</sup> )	$D_e = K_F/K_R$
Ext-PTFE	toluene	0.58	3.89	0.097	0.133	0.7
	n-hexane	0.52	4.17	0.103	0.061	1.7
	THF	0.72	5.11	0.128	0.055	2.3
	chloroform	0.25	11.1	0.279	0.094	3.0
SPS-PTFE	toluene	0.35	9.70	0.972	0.108	9.0
	n-hexane	0.16	5.00	0.500	0.089	5.6
	THF	0.29	3.33	0.333	0.094	3.5
	chloroform	0.34	4.45	0.446	0.110	4.0

511  
 512 This behavior can be related to the crystallinity of each sample. As mentioned in section 4.1,  
 513 the crystallinity of Ext-PTFE samples is higher than the SPS-PTFE counterparts. Thus, SPS-  
 514 PTFE is more subjected to redistribution of its free volume to provide additional sites and  
 515 accessibility to penetrant molecules, and consequently the relaxation process contribution in  
 516 sorption kinetics should be substantial. However, chains mobility is restricted in Ext-PTFE  
 517 due to its high crystallinity. As a result, transport of solvent into pre-existing and available  
 518 vacancies or sites of Ext-PTFE would be ensured mostly by Fickian diffusion contribution. A  
 519 direct comparison between time constants of diffusion and first order relaxation is provided  
 520 via the Deborah number  $De (= K_F/K_R)$  [55,56]. In our case, the  $D_e$  values are ranging from 1  
 521 and 10 which means that sorption kinetics is limited by polymer relaxation phenomenon.  
 522 Additionally, SPS-PTFE samples exhibit the highest characteristic times of diffusion  $K_F$   
 523 reflecting higher diffusion coefficients compared to Ext-PTFE samples. We note that this  
 524 trend corroborates the high equilibrium uptake of liquid by SPS-PTFE samples. The structural  
 525 features of each kind of samples can explain the observed differences in the  $D$  coefficient  
 526 values. The larger crystalline domains of Ext-PTFE samples constitute more obstacles to the  
 527 liquid diffusion paths and create an additional tortuosity that can delay diffusion according to  
 528 the expression  $D = D^*/(\zeta \beta_{imm})$ , where  $D^*$  is the diffusion coefficient in the bulk amorphous  
 529 polymer,  $\beta_{imm}$  is the chain immobilization factor that relates to the reduced mobility of the  
 530 polymer chains in the proximity of the crystals and  $\zeta$  is the tortuosity that accounts for the  
 531 increased diffusion path in order to bypass crystallites [29,55,57]. Additionally, the possible  
 532 existence of amorphous segments embedded in the crystals which constitute the rigid  
 533 amorphous fraction decreases and delays the transport of liquid molecules inside the polymer.

534

535 **4.5. Influence of liquid**

536

537 Among the prominent factors that can affect the absorbency of liquids by a polymer are the  
538 molar volume of solvents, density, and the chemical affinity with the polymer [29,50,57,58].

539 Table 1 outlines the relevant parameters of the liquids investigated. As mentioned above, the

540 equilibrium uptake  $Q_e$  of Ext-PTFE and SPS-PTFE increases in this order: toluene  $\leq$  n-

541 hexane  $\leq$  THF  $<$  chloroform. Additionally, the molar volume of toluene and n-hexane are higher

542 than those of THF and chloroform, thus the equilibrium uptake decreases as the molar volume

543 of the solvent molecule increases (Fig 8). In many studies dealing with semi-crystalline

544 polymers, it was observed that n-alkane and other elongated or flattened molecules like n-

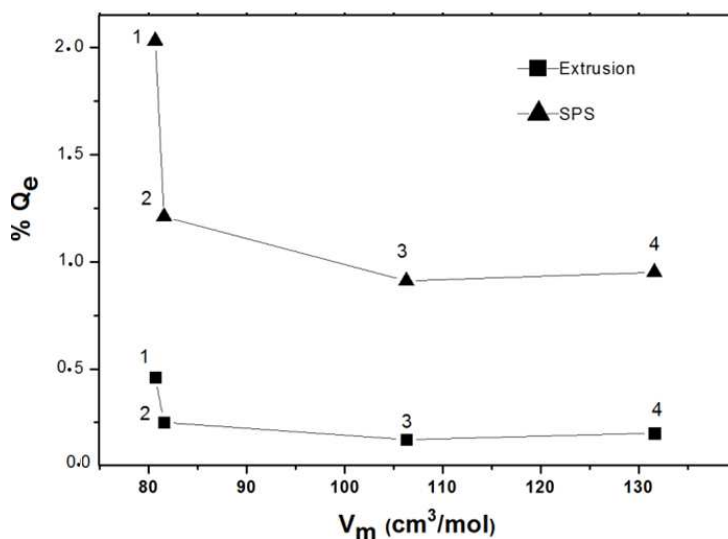
545 hexane are more accessible than spherical molecules of similar volume [29,50,59]. This

546 observation can provide an explanation why n-hexane is more absorbed than toluene even

547 though its molar volume is slightly larger. Similarly, chloroform which has the highest

548 density and the lowest molar volume can increase the equilibrium uptake by PTFE samples.

549



550

551

552 **Fig.8:** Plot showing the effect of liquid molar volume on uptake at saturation for PTFE

553 samples. (1): chloroform, (2): THF, (3): n-hexane, (4): toluene (solid lines are for guidance of

554 the eye).

555

556

557 According to the sorption results of PTFE and HSP approach, no correlation is evidenced

558 between the liquid equilibrium uptake by PTFE and the Hansen parameters for each liquid

559 investigated (Table 5). This conclusion corroborates prior studies [50,60] that have shown

560 equilibrium uptake by PTFE less than 1% for most hydrogen containing liquids and which

561 does not depend on the solubility parameters. Furthermore, the same references [50,60]  
562 reported that halogenated solvents penetrate more PTFE. This is what we observed for  
563 chloroform which has more chemical affinity with PTFE.

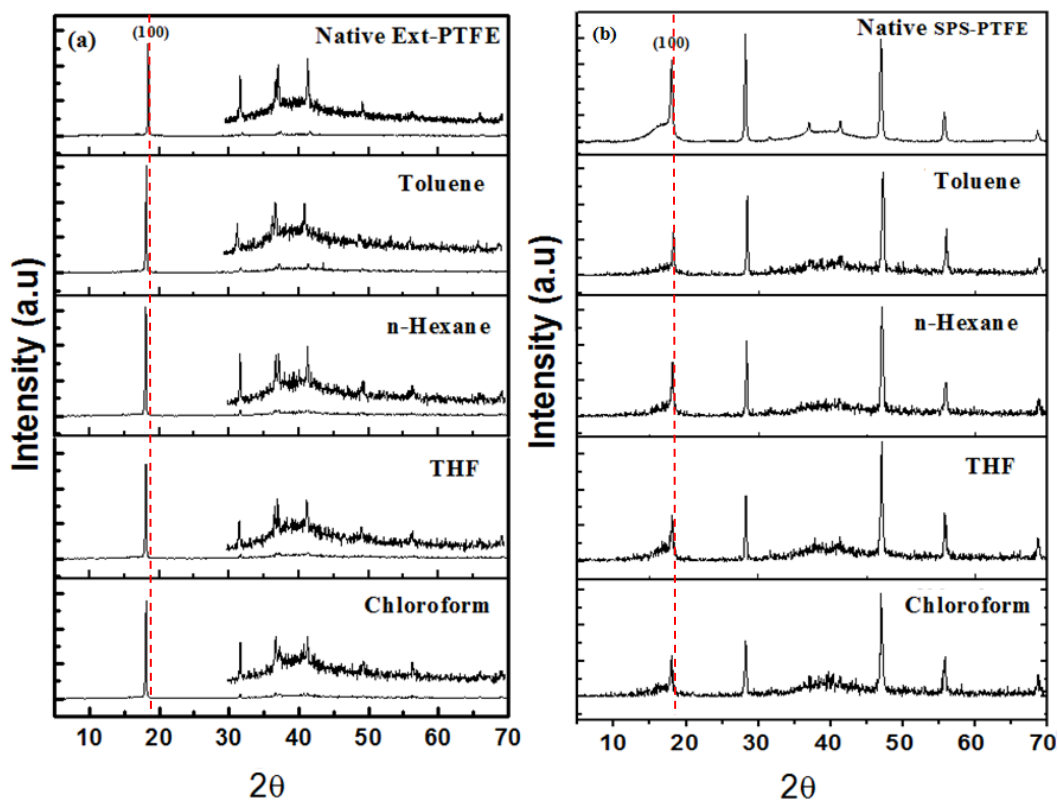
564

#### 565 **4.6. Structural characterization of swollen samples**

566

567 The effect of swelling on the polymer structural characteristics can be also inferred from the  
568 XRD pattern appearance. Figure 9(a) illustrates XRD patterns of native and swollen Ext-PTFE  
569 samples with a sharp peak at  $2\theta = 18.4^\circ$  and several weak peaks as well as two broad diffuse  
570 regions centered at  $16.5^\circ$  and  $39.7^\circ$ . Indexed peaks are shown in Table 8.

571 According to the temperature-pressure phase diagram, the phase behavior of PTFE is known  
572 to occur in four crystalline forms as reported by many studies [40,61,62]. At normal pressure  
573 and a temperature of  $19^\circ\text{C}$ , PTFE transforms form-II which is the triclinic structure to form-  
574 IV referring to the hexagonal lattice. The last form consists of hexagonally packed zigzag,  
575 twisted helices of linear chain polymeric molecules ( $-\text{CF}_2-\text{CF}_2-$ ). The transition form-II to  
576 form-IV consists of a decrease in screw frequency from  $13_6$  (13 units at 6 full spiral rotations)  
577 to  $15_7$ . At  $30^\circ\text{C}$ , form-IV transforms to I giving away to a pseudohexagonal structure, this  
578 conversion is considered to be a loss of ordering in the mutual-rotation of separate adjacent  
579 spirals. Forms II or I can be transformed to form III at high pressure (0.5 GPa) and high  
580 temperature ( $80^\circ\text{C}$ ) giving way to form a planar zigzag structure.



581

582 **Fig.9:** XRD patterns of (a) Ext-PTFE and (b) SPS-PTFE dry and swollen at equilibrium in  
 583 several liquids. The red dashed line shows the (100) peak.

584

585 Figure 9(b) presents XRD patterns of SPS-PTFE. Native SPS-PTFE exhibits the hexagonal  
 586 structure as Ext-PTFE. Nevertheless, several significant differences between both types of  
 587 samples can be observed: for SPS-PTFE, the (110) diffraction peak which is absent in the  
 588 XRD pattern of Ext-PTFE has the highest intensity; the (200) and (220) peaks do not appear  
 589 in the diffraction pattern; and the (210) peak has a strong intensity (Table 8). These disparities  
 590 originate from the preferred orientation and growth of crystal planes due to the processing  
 591 conditions [21,51] for Ext-PTFE and the interaction mechanisms between PTFE grains for  
 592 SPS-PTFE [62]. The XRD patterns of swollen Ext-PTFE samples keep general features with  
 593 non-swollen samples, but the (100) peak is slightly broadened and shifted to smaller angular  
 594 distances. For swollen SPS-PTFE, the three peaks around 37.3, 41.51° and 49.5°  
 595 corresponding to the (107), (108) and (210) peaks disappeared. Moreover, the (100) and (110)  
 596 peak intensities are weaker. The penetration of liquid into the polymer introduces disorder in  
 597 its crystalline structure by rotation of molecules segments  $(CF_2-CF_2)_n$  relative to each other  
 598 (twisting and untwisting) around and along the molecular axis. These features are in  
 599 agreement with those of an early theoretical modeling and experimental study of crystalline



600 ultra-dispersed PTFE powder [64]. In this paper, the authors concluded that a systematic  
 601 absence of (hkl) reflections with  $l \neq 0$  accompanied by broadening and intensity decrease of the  
 602 (100) peak can be related to molecular disorder around and along the molecular axis. The  
 603 broadening and shifting of the (100) peak to lower frequency was also observed by Liu *et al.*  
 604 [65] for irradiated PTFE with dose up to 4 MGy in oxygen at room temperature. This  
 605 investigation showed clearly the formation of new oxygen containing groups within the  
 606 structure of PTFE leading to lattice expansion and hindrance of the regular arrangement of  
 607 chain atom into the crystallite. Thus, the penetrant molecules change the lattice spacing and  
 608 induce a microstrain in the SPS-PTFE crystallites.

609 **Table 8:** XRD pattern attributions of Ext-PTFE and SPS-PTFE samples (S=sharp, W=weak,  
 610 VW=very weak, and M=moderate).

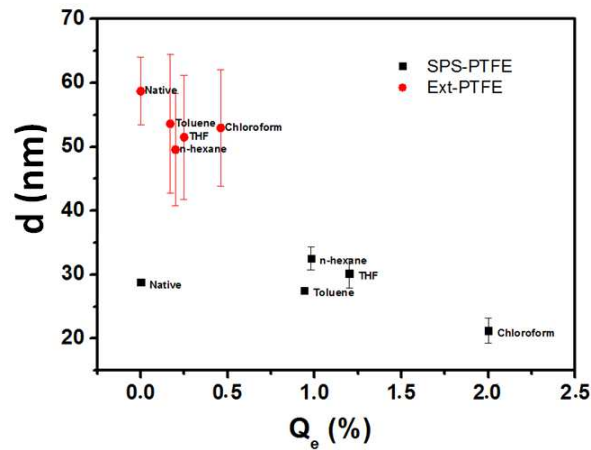
Miller index	Ext-PTFE		SPS-PTFE	
	peak	intensity	peak	intensity
100	18.4	S	18.0	M
110	-	-	28.2	VS
111	31.9	W	31.2	W
200	36	W	-	-
107	37.3	W	37.0	W
108	41.6	W	41.4	W
210	49.5	VW	47.0	S
300	56.6	VW	55.8	M
220	66.2	VW	-	-
310	69.4	VW	68.7	W
0015	72.9	VW	72.7	VW
1015	75.6	VW	75.8	W
halo diffusion	15	W	16.5	M
	40.1	W	39.6	M

623  
 624 Langford *et al.* [66] reported that the XRD line broadening is influenced by the apparent  
 625 crystallite sized which can be calculated by applying Debye-Scherrer's equation

$$d = \frac{k\lambda}{B \cos \theta} \quad (12),$$

628  
 629 where B (rad) is defined as full width at half-maximum (FWHM) of the (100) peak,  $k$  is the  
 630 Scherrer's constant (close to unity),  $\lambda$  is the wavelength of the irradiation, and  $\theta$  is the Bragg  
 631 angle between the incident ray and the diffraction pattern. The XRD data were fitted with a  
 632 convoluted Gaussian peak shape on a peak-by-peak basis using the software OriginPro 8.5.

633



634  
635

636 **Fig.10:** A plot reflecting the relationship between the apparent crystallite size of PTFE  
637 samples and the equilibrium uptake of several liquids.

638

639

640 Figure 10 shows the crystallite size of swollen and dry PTFE samples evaluated from Eq.(12).

641 For SPS-PTEF, it can be seen that the apparent crystalline size decreases as the equilibrium

642 uptake is increased. For Ext-PTFE, large error bars indicate that the crystalline domains were

643 weakly influenced by the liquid penetration.

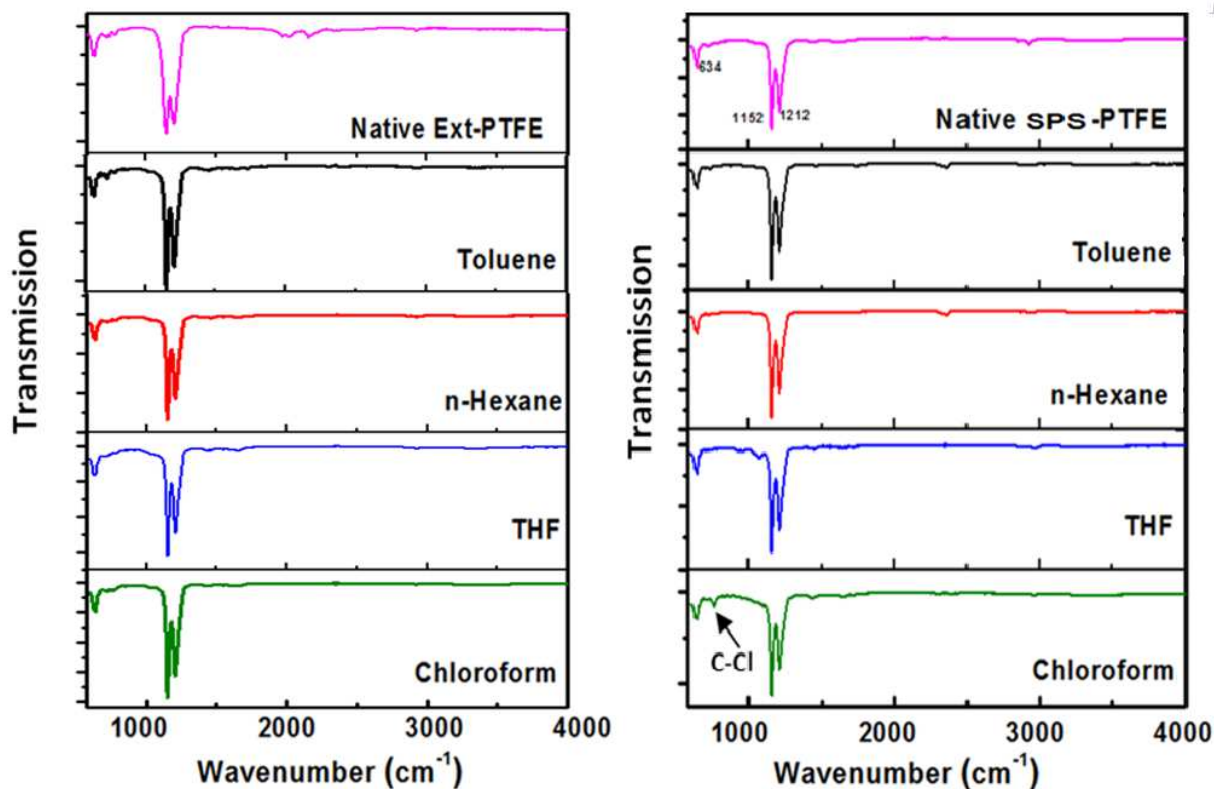
644

#### 645 4.7. FTIR analysis

646

647 The IR spectra of dry and swollen PTFE samples are shown in Fig.11.

648



**Fig.11:** FT-IR spectra of native PTFE and swollen Ext-PTFE and SPS-PTFE samples.

The IR spectra of dry and swollen PTFE samples are shown in Fig.11. In all spectra, the prominent IR peaks at 1150 and 1212  $\text{cm}^{-1}$  are related to the symmetric and asymmetric stretching modes of the  $\text{CF}_2$  groups [44,67-69]. Table 9 summarizes the IR band characteristics of samples and depicts differences between IR spectra of unswollen and swollen PTFEs. For the swollen SPS-PTFE spectra, the appearance of absorption bands related to CH,  $\text{CH}_2$ ,  $\text{CH}_3$  groups, and C-Cl is due to the penetrating liquids in the polymer phase [69]. For Ext-PTFE, no significant changes are observed in the IR spectra after swelling which is coherent with its small equilibrium uptake. Overall, these IR observations indicate that the pristine SPS-PTFE didn't experience chemical degradation from the SPS process and only the physisorption is involved for swollen polymer which corroborate the chemical inertia of the SPS-PTFE.

669 **Table 9:** Assignment of IR absorbance bands of swollen and native PTFE samples (W=weak,  
 670 VW=very weak, M=moderate, S=sharp).

671

IR band	Assignment	
	Native PTFEs	Swollen SPS-PTFE
620-640 W		CF deformation
718,765 VW		CF <sub>2</sub> scissoring
720-780 M	-	C-Cl stretching (SPS-PTFE swollen by chloroform)
1150, 1204-1210 S		CF <sub>2</sub> symmetric stretching
1436 W		C-F <sub>2</sub> asymmetric stretching
1456- 1462, 1621 W	-	CH <sub>2</sub> , CH <sub>3</sub> deformation
1580-1800 W	-	CH deformation
2918-2930 W, 2845 W	-	CH <sub>2</sub> , CH <sub>3</sub> stretching

672

673

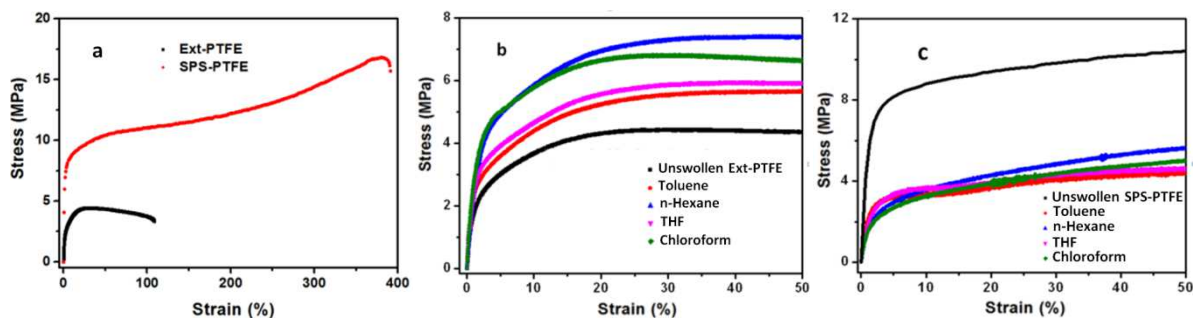
674 **4.8. Mechanical properties of swollen PTFEs**

675

676 Forces like compression or traction can induce a permanent deformation under swelling  
 677 conditions and eventually provoke mechanical failure of these materials [2,3,70-72]. Figure  
 678 12(a) shows the stress–strain relationships of dry PTFE samples. The main parameters  
 679 deduced from these experimental results are the Young’s modulus, yield stress, tensile  
 680 strength, and elongation at break (Table 10). For SPS-PTFE samples, these data reveal large  
 681 deformations at break up to ~390%, high elastic modulus and a better ductility compared to  
 682 the Ext-PTFE samples. A detailed interpretation of this behavior is beyond the scope of the  
 683 current study but is likely attributed to the high extent of fibrillation developed under stress  
 684 for SPS-PTFE samples leading to strong viscoelastic dissipation. Improving mechanical  
 685 properties of PTFE by SPS processing was reported in an earlier paper [15]. Besides, the  
 686 higher crystallinity of Ext-PTFE samples has for effect to increase its brittleness and decrease  
 687 its elongation at break. These observations are in agreement with those of Ridelli *et al.* [73]  
 688 who reported that high crystallinity reduces damping, **however** resulting also in an increase of  
 689 the elastic modulus. **Despite the higher crystallinity of Ext-PTFE compared to that of SPS-**  
 690 **PTFE, the latter is found to be more rigid and presents higher strength, ductility and**  
 691 **toughness. In an attempt to explain this behavior, we want note that similar trends have been**  
 692 **reported in Refs. [74-76]. For instance, F. Bedoui and coworkers [74] have demonstrated, on**  
 693 **the basis on a micromechanical model in which the semi-crystalline polymer material**  
 694 **microstructure is represented by crystalline inclusions embedded into an amorphous matrix,**  
 695 **the key importance of the inclusion aspect ratio (length over thickness), to explain a lower**  
 696 **modulus for HDPE ( $E=1200$  MPa,  $X_c= 70\%$ ) than for PP ( $E=1400$  MPa,  $X_c= 40\%$ )) despite a**

697 higher rigidity for both phases and a higher crystallinity for HDPE. Another report has  
 698 showed an increase of ultimate strength, elongation and toughness under uniaxial tension  
 699 when the crystallinity decreases for molded PTFE materials [75], suggesting that the  
 700 mechanical properties of semi-crystalline thermoplastic polymers are strongly microstructure-  
 701 dependant [77,78]. The complexity of this microstructure includes the differences in  
 702 molecular architecture of these materials, thermal treatment, and crystallization conditions.  
 703 For our samples, we believe that the aspect ratio of the crystalline phase for SPS-PTFE plays  
 704 a key role in enhancing the mechanical properties since the DSC thermograms of these  
 705 samples indicate the presence of ECC which are characterized by a high aspect ratio. The  
 706 sintering process contributes also to the observed mechanical properties of SPS-PTFE by  
 707 maintaining the compressive pressure at 25 MPa. This value is largely sufficient to provide an  
 708 effective compaction of PTFE particles since the room temperature yield strength of PTFE is  
 709 close to  $\sim 12.5$  MPa and decreases by increasing temperature [79]. Additionally, other  
 710 parameters such as the size of PTFE powder particles prior to processing, and distribution-  
 711 orientation-texture of crystalline phases, should be taken into account in order to fully  
 712 understand the differences between the mechanical responses of SPS- PTFE and Ext-PTFE  
 713 samples. Moreover, changing the load conditions, e.g DMA measurements by varying both  
 714 temperature and frequency, eventually bring additional information.

715



716

717

718 **Fig.12:** A plot of the stress-strain relationships of (a) unswollen PTFEs (b) Ext-PTFE and (c)

719

SPS-PTFE samples after swelling in different liquids: toluene, n-hexane, THF and

720

chloroform. Room temperature.

721

722 For swollen PTFE samples, Table 10 shows that the Young's modulus and yield stress of

723

SPS-PTFE decrease. The decreasing trend of these parameters with equilibrium uptake is also

724

observed for toluene, THF and chloroform. This can be explained by a polymer plasticization

725

by the liquid leading to a higher mobility of molecular chains and a weaker resistance to

726

deformation, in agreement with previous observations [70,79]. For Ext-PTFE, the opposite

727 trend is evidenced. The Young's modulus increases while the yield stress remains constant as  
 728 the equilibrium uptake increases with the notable exception of n-hexane. The presence of  
 729 solvent contributes to the decrease of the nanocrystallite size in Ext-PTFE samples during the  
 730 tensile tests. An early paper by Askadskii [80] showed that this change in the crystalline  
 731 structure of semi-crystalline polymers can be related to the Young's modulus increase.

732

733 **Table 10:** Young modulus and yield stress at elastic strain of 0.2% for Ext-PTFE and SPS-  
 734 PTFE(dry and equilibrium swollen) samples.

	Ext-PTFE		SPS-PTFE	
	$E$ (MPa)	$\sigma_e$ (MPa)	$E$ (MPa)	$\sigma_e$ (MPa)
dry	270	0.6	480	1
toluene	480	0.5	290	0.7
n-Hexane	274	0.5	184	0.4
THF	463	0.8	228	0.5
chloroform	412	0.8	200	0.5

735

736

## 737 5. Concluding remarks

738

739 We reported on the effect of swelling on the structural and mechanical properties of Ext-  
 740 PTFE and SPS-PTFE. The above results show that the sorption kinetics behavior of toluene,  
 741 n-hexane, tetrahydrofuran and chloroform are pseudo-Fickian. To rationalize the sorption  
 742 kinetics data the BH equation was used. Overall, we found that SPS-PTFE is characterized by  
 743 property gradients from the surface to the bulk and that the equilibrium uptake is larger than  
 744 for Ext-PTFE. An attempt was made to correlate the crystallinity of the native PTEFs deduced  
 745 from DSC, the equilibrium uptake for several liquids and the apparent diffusion coefficient, in  
 746 order to discriminate between the two kinds of samples explored. The combined effects of  
 747 free energy of the interface between the processed PTFE and liquid, the Hansen parameters  
 748 solubility, the molar volume and liquid type on the sorption rate are also discussed. It is found  
 749 that the lower crystallinity of SPS-PTFE, acting as a barrier to solvent diffusion, decreases its  
 750 resistance to swelling. XRD investigation exhibits a slight decrease in crystallite size in  
 751 swollen SPS-PTFE. Tensile experiments reveal that the native SPS-PTFE has the best  
 752 mechanical properties, and highlight a significant decrease of Young's modulus and yield  
 753 stress after swelling due to a plasticization effect. For Ext-PTFE samples, the opposite trend is  
 754 observed after swelling due to its higher crystallinity.

755

756

757

758 **Acknowledgements**

759 The authors thank the Center of Analysis of Cadi Ayyad University for FTIR and XRD  
 760 characterizations. We gratefully acknowledge the assistance of G. Bonnefont for SPS  
 761 experiments.

762  
 763 **Appendix A**

764  
 765 The dispersive and polar components of both Ext-PTFE and SPS-PTFE samples are  
 766 calculated by applying Owen-Wendt’s model and using contact angle measurements. We  
 767 proceed by linear regression which permits to evaluate correctly the errors involved. The

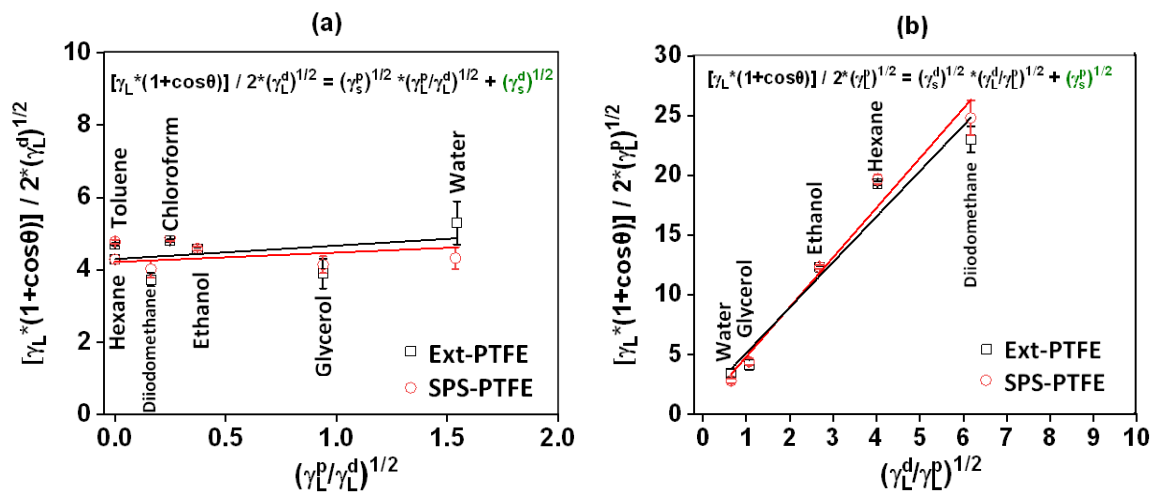
768 points on the x- and y-axis are calculated for each solvent using  $x = \left(\frac{\gamma_L^p}{\gamma_L^d}\right)^{1/2}$ ,  $y = \frac{\gamma_L(1 + \cos \theta)}{2(\gamma_L^d)^{1/2}}$

769 as shown in Fig. 13(a). Then, regression calculates  $\gamma_s^p = a^2$  and  $\gamma_s^d = b^2$ . By plotting

770  $y = \frac{\gamma_L(1 + \cos \theta)}{2(\gamma_L^d)^{1/2}}$  versus  $x = \left(\frac{\gamma_L^d}{\gamma_L^p}\right)^{1/2}$  (Fig. 13(b)), we obtain the intercept on the y-axis which

771 corresponds to  $(\gamma_L^p)^{1/2}$  and the slope  $(\gamma_L^d)^{1/2}$ . Only the positive solutions with smallest average  
 772 deviation are selected.

773



774  
 775

776 **Fig.13:** Linear regression analysis of contact angle measurement for the different solvents and  
 777 PTFE samples explored.

778 **Funding**

779 This research did not receive any specific grant from funding agencies in the public,  
 780 commercial, or not-for-profit sectors.

781

782 **References**

783

- 784 [1] Polytetrafluoroethylene (PTFE) Market Report, Trends, Forecast and Competitive  
785 Analysis, Lucintel, Report linker, ID: 5308395, Vol: January 2018.  
786 <https://www.reportlinker.com/p05308395>
- 787 [2] E. Burkarter, C. K. Saul, F. Thomazi, N. C. Cruz, L.S. Roman, W. H. Schreiner,  
788 Superhydrophobic electrosprayed PTFE, *Surf.Coat.Tech.* 202(1), (2007)194–198.  
789 <https://doi.org/10.1016/j.surfcoat.2007.05.012>
- 790 [3] E. Dhanumalayan, M. G Joshi, Performance properties and applications of  
791 polytetrafluoroethylene (PTFE) - a review, *Adv.Compos.Hybrid.Mater.* 1(2)(2018)  
792 247–268. <https://doi.org/10.1007/s42114-018-0023-8>
- 793 [4] L. K. Massey, *Polytertrafluoroethylene*, in: L. K. Massey (Ed), *Permeability properties*  
794 *of plastics and elastomers: a guide to packaging and barrier materials*, Second ed.,  
795 *Plastic design library.*, USA, 2003, pp: 101-108.
- 796 [5] D. Troy, Remington, *The Science and Practice of Pharmacy*, 21st ed., Lippincott  
797 *Williams and Willkins.*, USA, 2005.
- 798 [6] W. -E. Liewellyn, J.-F. Lontz, Extrusion of Tetrafluoroethylene polymer, US Patent:  
799 2,685,707 (1950).
- 800 [7] S. Hambir and J. P. Jog, Sintering of ultrahigh molecular weight polyethylene, *Bull.*  
801 *Mater.Sci.* 23(3) (2000)221-226. <https://doi.org/10.1007/BF02719914>
- 802 [8] X. Colin and J. Verdu, Polymer degradation during processing, *C. R. Chimie.* 9 (2006)  
803 1380–1395. <https://doi.org/10.1016/j.crci.2006.06.004>
- 804 [9] A.–M. M. Baker, C. M. Barry, Effect of composition, processing, and structure on  
805 properties of engineering Plastics, in: S. Lampman (Ed), *Characterization and failure*  
806 *analysis of plastics, Materials selection and design*, Volume 20, *ASM Handbook*, ASM  
807 International, 2003, USA, p. 28.
- 808 [10] M. Suárez, A. Fernández, J. L. Menendez, R. Torrecillas, H. U. Kessel, J. Henicke, R.  
809 Kirchner, T. Kessel, Challenges and Opportunities for Spark Plasma Sintering: A key  
810 Technology for a New Generation of Materials, in: B. Ertu (Ed), *Sintering Applications*,  
811 *InTech.*, Croatia, 2013, pp. 319–342.
- 812 [11] P. Cavaliere, B. Sadeghi, A. Shabani, Spark Plasma Sintering: Process Fundamentals,  
813 in: P. Cavaliere (Ed), *Spark Plasma Sintering of Materials Advances in Processing and*  
814 *Applications*, Springer Cham., Switzerland , 2019, pp. 3 - 21.



- 815 [12] H. Huang, X. Yu, Automated industrial PTFE billet sintering temperature profile  
816 optimization for residual stress reduction, SIMULIA Community Conference, May 15-  
817 17, 2012 - Providence RI, USA
- 818 [13] L. Andena, M. Rink, F. Polastri, Simulation of PTFE sintering: Thermal stresses and  
819 deformation behavior, *Polym. Eng. Sci.* 44 (2004) 1368–1378.  
820 <https://doi.org/10.1002/pen.20132>
- 821 [14] R. B. Canto, N. Shmitt, J. De Carvalho, R. Billardon, Experimental identification of the  
822 deformation mechanisms during sintering of cold compacted polytetrafluoroethylene  
823 powders, *Polym.Eng.Sci.* 51(11) (2011) 2220–2235. <https://doi.org/10.1002/pen.21994>
- 824 [15] A. Mdarhri, I. Elaboudi, , O. Lame, D. Fabregue, C. Brosseau, A. Nourdine, G.  
825 Bonnefont, Processing, microstructure and mechanical analysis of  
826 Polytetrafluoroethylene sintered by field assisting sintering technique, in the press.
- 827 [16] J-C. Sebileau, S. Lemonnier, E. Barraud, M-F. Vallat, A. Carrado, M. Nardin,  
828 Consolidation by spark plasma sintering (SPS) of PEEK, *J.Appl.Polym.Sci.* 134 (2017)  
829 44911. <https://doi.org/10.1002/app.44911>
- 830 [17] M. Schwertz, S. Lemonnier, E. Barraud, A. Carrado, M. Nardin, Consolidation by spark  
831 plasma sintering of polyimide and polyetheretherketone, *J. Appl. Polym.Sci.* 131  
832 (2014) 40783. <https://doi.org/10.1002/app.40783>
- 833 [18] M. Schwertz, P. Ranque, S. Lemonnier, E. Barraud, A. Carrad, M. F. Vallat, M. Nardin,  
834 Optimization of the Spark Plasma Sintering Processing Parameters Affecting the  
835 Properties of Polyimide, *J. Appl. Polym. Sci.* 132 (2014) 41542.  
836 <https://doi.org/10.1002/app.41542>
- 837 [19] K. Wei, G-S.Nolas, Enhanced thermoelectric properties of polymer/inorganic bulk  
838 composites through EG treatment and spark plasma sintering processing, *Scripta.Mater.*  
839 150 (2018) 70-73.
- 840 [20] H. Lahlali, A. Mdarhri, M. Zaghrioui, F. El Haouzi, I. El Aboudi and M. El Azhari, A  
841 high viscous polymer processed by conventional and unconventional techniques:  
842 evaluation of mechanical behaviour and physical characteristics, *Adv. Mater.*  
843 *Process.Technol.* 3 (2017) 196-205. <https://doi.org/10.1080/2374068X.2016.1247238>
- 844 [21] S-I. Manabe, Supermolecular structure of polymer solids and its effects on penetrant  
845 transport, in: P. Neogi (Ed), *Diffusion in Polymers*, Marcel Dekker Inc., New York,  
846 1996, pp.211-250.

- 847 [22] M. Chainey, Transport phenomena in polymer films, in: N. P. Cheremisinoff (Ed),  
848 Handbook of polymer chain and technology: v.4 composites and specialty applications,  
849 Marcel Dekker Inc., New York, 1989, pp. 499-540.
- 850 [23] A. R. Berens, H. B. Hopfenberg, Diffusion and relaxation in glassy polymer powders: 2.  
851 Separation of diffusion and relaxation parameters, *Polymer*. 19 (1978) 489-496.  
852 [https://doi.org/10.1016/0032-3861\(78\)90269-0](https://doi.org/10.1016/0032-3861(78)90269-0)
- 853 [24] H-C. Van Ness, M-M. Abbott, Thermodynamics in: D-W. Green, R-H. Perry (Eds),  
854 Perry's Chemical Engineer's Handbook, eighth ed., The McGraw-Hill Companies.,  
855 USA, 2008, pp. 1-40.
- 856 [25] DuPont-Fluoroproducts, Teflon, PTFE, properties handbook, Tech. Rep. H-37051-3,  
857 DuPont, 1996.
- 858 [26] J. Cranck, The mathematics of diffusion, Second ed., Oxford University Press, Oxford,  
859 1975.
- 860 [27] P-L. Ritger, N-A. Peppas, A simple equation for description of solute release I. Fickian  
861 and non-Fickian release from non-swellable devices in the form of slabs, spheres,  
862 cylinders and discs, *J. Control.Release*. 5 (1987) 23-26. [https://doi.org/10.1016/0168-](https://doi.org/10.1016/0168-3659(87)90034-4)  
863 [3659\(87\)90034-4](https://doi.org/10.1016/0168-3659(87)90034-4)
- 864 [28] M. M. Wind, H. J. W. Lenderink, A capacitance study of pseudo-Fickian diffusion in  
865 glassy polymer coatings, *Prog.Org.Coat.* 28 (1996) 239-250.  
866 [https://doi.org/10.1016/0300-9440\(95\)00601-X](https://doi.org/10.1016/0300-9440(95)00601-X)
- 867 [29] C, E, Roger, Permeation of Gases and Vapours in Polymers, in: J. Comyn (Ed),  
868 Polymer permeability, Elsevier Applied Science., London, 1985, p.11-69.
- 869 [30] H. L. Frisch, Sorption and Transport in Glassy Polymers-A Review, *Polym.Eng.Sci.* 20  
870 (1980) 2-13. <https://doi.org/10.1002/pen.760200103>
- 871 [31] A. R. Berens, H. B. Hopfenberg, Diffusion of organic vapors at low concentrations in  
872 glassy PVC, polystyrene, and PMMA, *J.Memb.Sci.* 10 (1982) 283-303.  
873 [https://doi.org/10.1016/S0376-7388\(00\)81415-5](https://doi.org/10.1016/S0376-7388(00)81415-5)
- 874 [32] S- K. Burgess, D-S. Mikkilineni, D- B. Yu, D- J. Kim, C- R. Mubarak, R- M. Krieger,  
875 W- J. Koros, Water sorption in poly(ethylene furanoate) compared to poly(ethylene  
876 terephthalate). Part 2: Kinetic sorption, *Polymer*. 55 (26) (2014) 6861-6869.  
877 <https://doi.org/10.1016/j.polymer.2014.10.047>  
878
- 879 [33] Y. P. Khanna, The melting temperature of polytetrafluoroethylene, *J.Mater.Sci.Lett.* 7  
(1988) 817-818. <https://doi.org/10.1007/BF00723770>

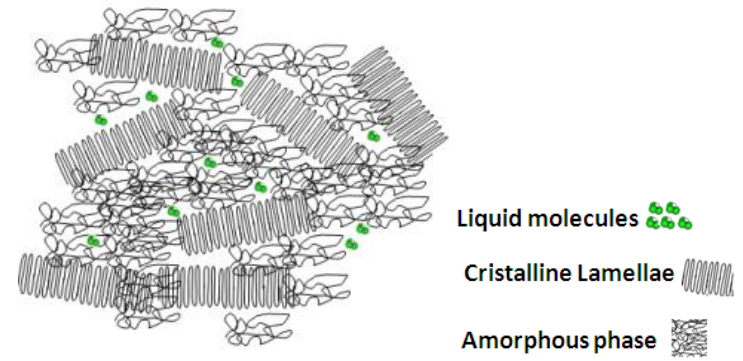
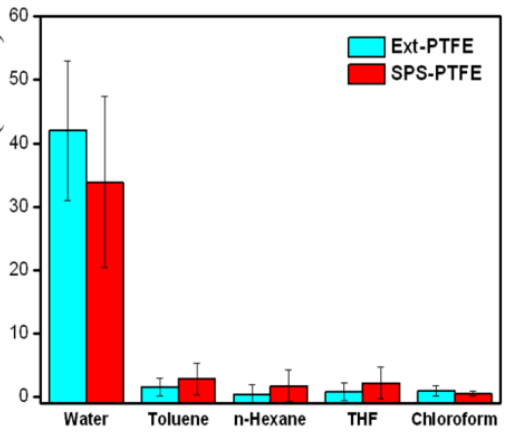
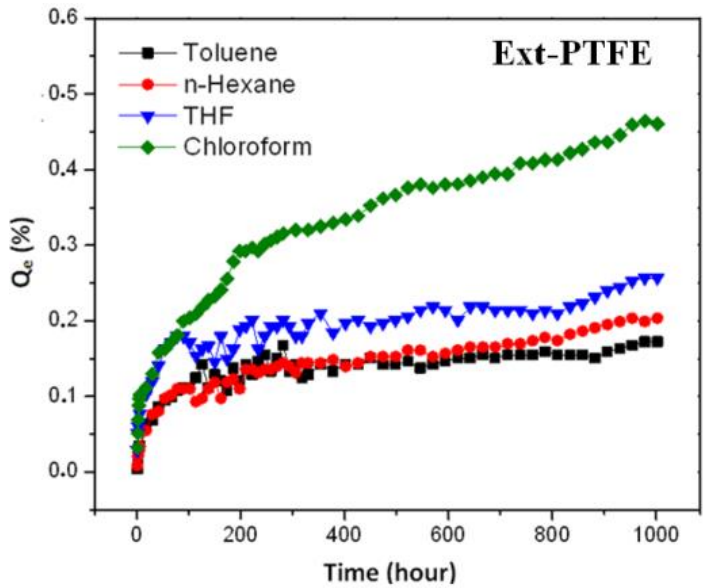
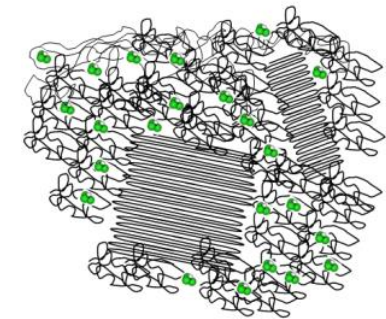
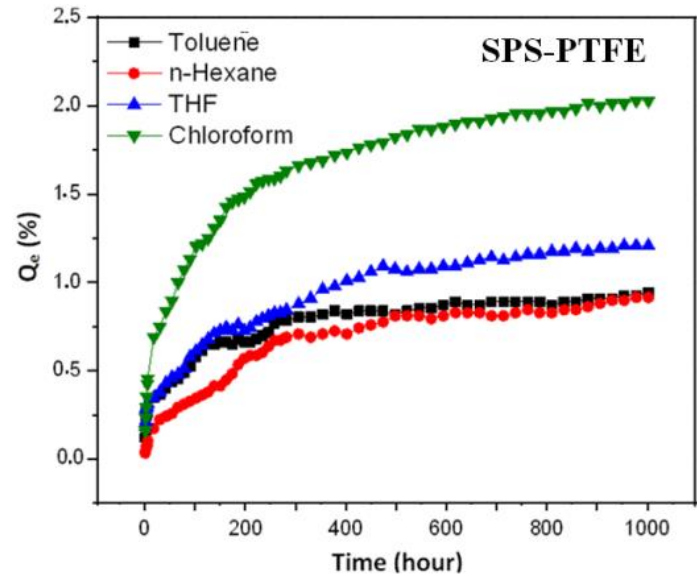
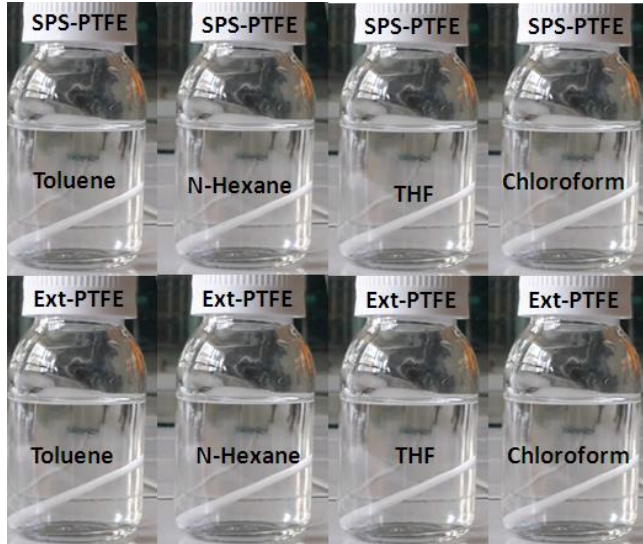
- 880 [34] F. Lui, T. Sun, P. Tang, H. Zhang, F. Qui, Understanding chain folding morphology of  
881 semicrystalline polymers based on a rod-coil multiblock model, *Soft Matter*,13 (2017)  
882 8250–8263. <https://doi.org/10.1039/C7SM01892D>
- 883 [35] S. A. Serov, S. A. Khatipov, N. V. Sadovskaya, A. V. Tereshenkov, N. A. Chukov,  
884 Double melting in polytetrafluoroethylene  $\gamma$ -irradiated above its melting point,  
885 *Nucl.Instrum.Meth.B.* 271 (2012) 92–95. <https://doi.org/10.1016/j.nimb.2011.11.003>
- 886 [36] A. Oshima, Y. Tabata, H. Kudoh, T. Seguchi, Radiation induced crosslinking of  
887 Polytetrafluoroethylene, *Radiat. Phys. Chem.* 45 (1995) 269–273.  
888 [https://doi.org/10.1016/S0969-806X\(96\)00189-2](https://doi.org/10.1016/S0969-806X(96)00189-2)
- 889 [37] B. Wunderlich, *Thermal Analysis of Polymeric Materials*, Springer., Berlin, 2005.
- 890 [38] M. Shimizu, C. Ikeda, M. Matsuo, Development of high-modulus and high-strength  
891 poly(tetrafluoroethylene) fibers by elongation at a liquid crystalline state, *Macromolecules.* 29  
892 (1996) 6724–6729. <https://doi.org/10.1021/ma951790d>
- 893 [39] R-L. Blaine, Thermal applications note polymer heats of fusion, TN048, TA  
894 Instruments.
- 895 [40] J. E. Mark, *Polymer Data Handbook*, Oxford University Press. Inc., Oxford, 1999.
- 896 [41] S. Chen, J. Wang, T. Ma, and D. Chen, Molecular dynamics simulations of wetting  
897 behavior of water droplets on polytetrafluorethylene surfaces, *J. Chem. Phys.*140 (2014)  
898 114704. <https://doi.org/10.1063/1.4868641>
- 899 [42] Y. Yuan, T. R. Lee, Contact Angle and Wetting Properties, in: G. Bracco, B. Holst  
900 (Eds.), *Surface Science Techniques: Springer Series in Surface Sciences*, Volume 51,  
901 Springer., Berlin and Heidelberg, 2013, pp. 3-34
- 902 [43] D. K. Owens, R. C. Wendt, Estimation of the surface free energy of polymers,  
903 *J.App.Poly.Sci.* 13 (1969) 1741-1747. <https://doi.org/10.1002/app.1969.070130815>
- 904 [44] J. H. Clint, Adhesion under water: surface energy considerations, *Int.J.Adhes.* 21  
905 (2001)267-273. [https://doi.org/10.1016/S0143-7496\(00\)00029-4](https://doi.org/10.1016/S0143-7496(00)00029-4)
- 906 [45] M.L. Gonzalez-Martin, B. Jańczuk, L. Labajos-Broncano, J. M. Bruque, Determination  
907 of the Carbon Black Surface Free Energy Components from the Heat of Immersion  
908 Measurements, *Langmuir.* 13 (1997) 5991. <https://doi.org/10.1021/la9621224>
- 909 [46] M. Żenkiewicz, Methods for the calculation of surface free energy of solids,  
910 *J.Achiev.Mater.Manuf.Eng.* 24 (2007) 137-145.
- 911 [47] C.M. Hansen, Polymer additives and solubility parameters, *Prog.Organ.Coat.* 51 (2014)  
912 109–112. <https://doi.org/10.1016/j.porgcoat.2004.05.003>

- 913 [48] A. Falsafi, S. Mangipudi, M. J. Owen, Surface and interfacial properties, in: J.E. Mark  
914 (Ed.), *Physical Properties of Polymers Handbook*, Springer Science and Business Media  
915 LLC., 2007, pp. 1011-1020.
- 916 [49] Y. Katasho, Y. Liang, S. Murata, Y. Fukunaka, T. Matsuok, S. Takahash, Mechanisms  
917 for Enhanced Hydrophobicity by Atomic-Scale Roughness, *Sci. Rep.* 5 (2015) N 13790.  
918 <https://doi.org/10.1038/srep13790>
- 919 [50] C. M. Hansen, *Hansen Solubility Parameters: A User's Handbook*, second ed., CRC  
920 Press, Taylors & Francis Group, London and New-York, 2007.
- 921 [51] S. Ebnesajjad, P. R. Khaladkar, Properties of Neat (Unfilled) and Filled  
922 Fluoropolymers, in: S. Ebnesajjad, P-R. Khaladkar (Eds.), *Fluoropolymers applications*  
923 *in Chemical Processing Industries, The definitive User's Guide and Databook*, William  
924 Andrew publishing., Norwich, NY ,2005, pp.17-128.
- 925 [52] C. M. Hansen, L. Just, Prediction of environmental stress cracking in Plastics with  
926 Hansen solubility parameters, *Ind. Eng. Chem. Res.* 40 (1) (2001) 21-25.  
927 <https://doi.org/10.1021/ie9904955>
- 928 [53] B. K. Storm, Surface protection and coatings for wind turbine rotor blades, in: P.  
929 Brøndsted, R-P.L. Nijssen (Eds.), *Advances in Wind Turbine Blade Design and*  
930 *Materials*, Woodhead Publishing Series in Energy No 47., 2013, pp. 387-412.
- 931 [54] M. Sabard, F. Gouanve, E. Espuche, R. Fulchiron, G. Seytre, L-A. Fillot, L. Trouillet-  
932 Fonti, Influence of film processing conditions on the morphology of polyamide  
933 6:Consequences on water and ethanol sorption properties, *J.Membr. Sci.* 415–416  
934 (2012) 670–680.
- 935 [55] SK. Burgess, RM. Kriegel, WJ. Koros, Diffusion coefficient modeling in polyester  
936 barrier materials: applications of infinite series solutions. Society of Plastics Engineers –  
937 ANTEC, 2014, Las Vegas, Nevada: p. 830-835.
- 938 [56] J-S.Vrentas, C-M. Jarzebski, J-L. Duda, A Deborah number for diffusion in polymer  
939 solvent systems, *J.AICHe.* 21(5) (1975) 894-901. <https://doi.org/10.1002/aic.690210510>
- 940 [57] A. S. Michaels, R. B. Parker JR, Sorption and flow of gases in polyethylene,  
941 *J.Polym.Sci.* 41 (1959) 53-71. <https://doi.org/10.1002/pol.1959.1204113805>
- 942 [58] X. Q. Cheng, Y. L. Zhang, Z. X. Wang, Z. Hu. Guo, Y. P. Bai, L. Shao, Recent  
943 Advances in Polymeric Solvent-Resistant Nanofiltration Membranes,  
944 *Adv.Polym.Technol.* 33 (S1) (2014) 21455. <https://doi.org/10.1002/adv.21455>
- 945 [59] A. Aitkin, R. M. Barraer, Transport and solubility of isomeric paraffins in rubber, *Trans.*  
946 *Faraday.Soc.* 51 (1955) 116-130. <https://doi.org/10.1039/TF9555100116>

- 947 [60] S. Ebnesajjad, Fluoropolymers: Properties and Structure, in: S. Ebnesajjad (ed.),  
948 Fluoroplastics, Volume 1: Non-Melt Processible Fluoropolymers - The definitive User's  
949 Guide and Data book, William Andrew-Elsevier., Oxford and Waltham, 2015, pp. 39-  
950 45.
- 951 [61] C. W. Bunn, E. R. Howells, Structures of Molecules and Crystals of Fluoro-Carbons,  
952 Nature. 174 (1954) 549–551. <https://doi.org/10.1038/174549a0>
- 953 [62] E. N. Brown, D. M. Dattelbaum, The role of crystalline phase on fracture and  
954 microstructure evolution of polytetrafluoroethylene (PTFE), Polymer. 46(9) (2005)  
955 3056-3068. <https://doi.org/10.1016/j.polymer.2005.01.061>
- 956 [63] C. W. Bunn, D. R. Holmes, “Chain configurations in crystals of simple linear  
957 polymers”, Discuss. Faraday.Soc. 25 (1958) 95-103. [https://doi.org](https://doi.org/10.1039/DF9582500095)  
958 /10.1039/DF9582500095
- 959 [64] V. M. Bouznik, S. D. Kirik, L. A. Solovyov, A. K. Tsvetnikov, A crystal structure of  
960 ultra-dispersed form of Polytetrafluoroethylene based on X-ray powder diffraction data,  
961 Powder.Diffr. 19(3) (2004) 219-224. <https://doi.org/10.1154/1.1707037>
- 962 [65] S. Liu, C. Fu, A. Gu, Z. Yu, Structural changes of Polytetrafluoroethylene during  
963 irradiation in oxygen, Radiat. Phys. Chem. 109 (2015) 1-5.  
964 <https://doi.org/10.1016/j.radphyschem.2014.12.005>
- 965 [66] J. I. Langford, A. J. C. Wilson, Scherrer after sixty years: A survey and some new  
966 results in the determination of crystallite size, J Appl.Crystallogr. 11 (1978) 102–103.  
967 <https://doi.org/10.1107/S0021889878012844>
- 968 [67] J. Mihaly, S. Sterkel, H. M. Ortner, L. Kocsis, L. Hajba, E. Furdyga, J. Mink, FTIR and  
969 FT-Raman Spectroscopy Study on polymer based high pressure digestion vessels,  
970 CCACAA. 79(3) (2006) 497-501.
- 971 [68] G-S. Kang, H-J. Ko, C-K. Choi, Chemical band structure of a-C:F films with low  
972 dielectric constant deposited by using CH<sub>4</sub>/CF<sub>4</sub> IPCVD, J. Korean.Phys.Soc. 42(5)  
973 (2003) 676-681.
- 974 [69] V. Sablinskas, G. Steiner, M. Hof, Applications, in: G. Gauglitz, T. V-Dinh (Eds).,  
975 Handbook of Spectroscopy, Wiley-VCH Verlag GmbH & Co. KGaA, Weinheim., 2014,  
976 pp. 89-112.
- 977 [70] S. Ebnesajjad, History of Polytetrafluoroethylene and expanded PTFE membrane, in: S.  
978 Ebnesajjad (ed.), Expanded PTFE Applications Handbook: Technology, Manufacturing  
979 and Applications, William Andrew-Elsevier, Oxford and Cambridge., 2017, pp.1-8.

- 980 [71] S. Lampman, Mechanical behavior and Wear, in: S. Lampman (ed.), Characterization  
981 and failure analysis of plastics, ASM International., USA, 2003, pp.183-292.
- 982 [72] C. A. Daniels, Tensile Properties, in: C. A. Daniels (ed.), Polymers: Structure and  
983 Properties, Technomoc Publishing company., Lancaster and Basel, 1989, pp. 43-56.
- 984 [73] M. N. Riddell, P. Koo, J. L. O'Toole, Fatigue mechanisms of thermoplastics,  
985 Polym.Eng.Sci. 6 (1966) 363-368. <https://doi.org/10.1002/pen.760060414>
- 986 [74] F. Bedouia, J. Diani, G. Regnier, Micromechanical modelling of elastic properties in  
987 Polyolefins, Polymer. 45(7) (2004) 2433–2442.  
988 <https://doi.org/10.1016/j.polymer.2004.01.028>
- 989 [75] T-Y. Hu, N. S. Eiss, The effects of molecular weight and cooling rate on fine  
990 structure, stress-strain behavior and wear of Polytetrafluoroethylene, J. Wear. 84 (1983)  
991 203 – 215. [https://doi.org/10.1016/0043-1648\(83\)90264-8](https://doi.org/10.1016/0043-1648(83)90264-8)
- 992 [76] P-E. Thomas, J-F. Lontz, C-A. Sperati, J-L. McPherson, Effects of fabrication on the  
993 properties of Teflon resins, Soc. Plast. J. 12 (1956) 89-95.
- 994 [77] S. Humbert, O. Lame, R. Séguéla, G. Vigier. A re-examination of the elastic modulus  
995 dependence on crystallinity in semi-crystalline polymers. Polymer. 52 (2011)  
996 4899-4909. <https://doi.org/10.1016/j.polymer.2011.07.060>
- 997 [78] L. Chazeau, C. Gauthier, G. Vigierand, J.-V. Cavallé, Relationships between  
998 Microstructural Aspects and Mechanical Properties, in: H.S. Nalwa (ed.), Handbook of  
999 Organic-Inorganic Hybrid Materials and Nanocomposites Volume 2, American  
1000 Scientific Publishers., California, 2003, pp. 63-109.
- 1001 [79] P-Y. Le Gac, M. Arhant, M. Le Gall, P. Davies, Yield stress changes induced by water  
1002 in polyamide 6: Characterization and modeling, Polym.Degrad.Stab. 137 (2017) 272-  
1003 280. <https://doi.org/10.1016/j.polymdegradstab.2017.02.003>
- 1004 [80] A. Askadskii, M. Popova, T. Matseevich, E. Afanasyev, The Influence of the degree of  
1005 crystallinity on the elasticity modulus of polymers, Adv. Mater.Res. 864-867 (2014)  
1006 640-643. <https://doi.org/10.4028/www.scientific.net/AMR.864-867.640>

1007  
1008



Sorption kinetics of poly-tetrafluoroethylene processed either by extrusion (Ext-PTFE) or spark plasma sintering (SPS-PTFE). Effect of crystallinity and interfacial free energy on sorption kinetic and equilibrium swelling ratio  $Q_e$